

FACULTAD DE INGENIERÍA UNIVERSIDAD NACIONAL
DE MAR DEL PLATA

**Sistemas Complejos, Ruidos
Discretos y su implementación en
FPGA**

TESIS

PARA OBTENER EL TÍTULO DE

DOCTOR EN INGENIERÍA CON ORIENTACIÓN EN ELECTRÓNICA

MAXIMILIANO ANTONELLI

DEDICATORIA

Agradecimientos

¡Muchas gracias a todos!

Índice general

1. Introducción	1
2. Generadores de Números Aleatorios	3
2.1. Cripto-Codificación caótica Variante en el tiempo	3
2.1.1. Introducción	3
2.1.2. Mapas cuadráticos bidimensionales	4
2.1.3. Implementación	4
2.1.4. Resultados	9
2.2. Codificación variable en el tiempo empleando mapa caótico (póster CASE2012)	10
2.3. Estudio del Caos en Redes Neuronales Discretas para su Implementación en Hardware (Informe Inteligencia computacional, Poster CASE2014)	11
2.4. <i>RO-based PRNG: FPGA implementation and stochastic analysis</i> .	12
2.4.1. Introduction	12
2.4.2. Hardware implementation.	13
2.4.3. Quantifiers	17
2.4.4. Results	18
2.4.5. Conclusions	21
2.5. Implementación de algoritmo genético para la búsqueda automática de caos en sistemas multiatractores (póster CASE2013)	21
3. Cuantificadores de Aleatoriedad	23
3.1. Implementación de algoritmo genético para la búsqueda automática de caos (Póster CASE 2013)	23
3.2. Hardware Implementation of Maximum Lyapunov Exponent . . .	24
3.2.1. Introduction	24
3.2.2. Maximum Lyapunov exponent	24
3.2.3. Chaotic System analyzed	25

3.2.4. Design of the System	27
3.2.5. Results	28
3.2.6. Conclusions	28
3.3. Causal and Non-causal Entropy quantifiers implemented in FPGA	32
3.3.1. Introduction	32
3.3.2. Causal and Non causal Entropy	33
3.3.3. Implemented Hardware	34
3.3.4. Implemented Software	37
3.3.5. Results	39
3.3.6. Discussion	40
3.3.7. Conclusions and future work	41
3.4. Measuring the Jitter of Ring Oscillators by means of Information Theory Quantifiers	42
3.4.1. Introduction	42
3.4.2. Determination of jitter in <i>RO</i> 's	44
3.4.3. Information Theory Quantifiers	45
3.4.4. Results	51
3.4.5. Conclusions	60
4. El problema de la Aritmética Discreta	63
4.1. Analysis of the digital implementation of a chaotic deterministic-stochastic attractor (EAMTA 2012)	63
4.2. Complexity of switching chaotic maps	64
4.2.1. Introduction	64
4.2.2. Information theory quantifiers	65
4.2.3. Results	69
4.2.4. Simple maps.	69
4.2.5. Conclusions	74
5. Conclusiones	85
A. Field Programmable Gate Array (FPGA)	87
Bibliografía	89

Capítulo 1

Introducción

Aqhora arranco con todo...

Capítulo 2

Generadores de Números Aleatorios

2.1. Cripto-Codificación caótica Variante en el tiempo

2.1.1. Introducción

En los sistemas de comunicaciones y particularmente en los dedicados a la codificación para el control de error y encriptamiento de datos se usan técnicas derivadas de la teoría de señales. Estas técnicas se aplican típicamente en la forma lineal debido a la simplicidad que ésto trae aparejado. Además cada una se implementa algorítmicamente o físicamente como una entidad independiente. Para cada sistema en particular se las elige con criterios de conveniencia práctica, y se las aplica en forma consecutiva o encadenada. La teoría de los sistemas no lineales [?, ?] aparece como un marco de trabajo ideal para ser utilizado en el contexto anteriormente mencionado. La existencia de los sistemas caóticos, y la relación de estos con la aleatoriedad, o pseudo aleatoriedad, otorga una plataforma de diseño que hasta hoy se encuentra poco explotada.

En los últimos veinte años se han presentado diversos trabajos que emplean caos en los sistemas de comunicaciones, como por ejemplo el empleo de portadoras caóticas sincronizadas en las transmisiones analógicas [?, ?]. Si nos centramos en la representación discreta un referente muy importante es el excelente trabajo de Kozic et. als. [?, ?] en el que se presenta una técnica de modulación empleando mapas caóticos unidimensionales lineales por tramos, la técnica consiste en la introducción del mensaje a codificar en el bit menos significativo de la secuencia

generada. Obteniéndose una secuencia levemente alterada lo que impide que el sistema entre en ciclos periódicos.

En este trabajo se propone un grupo de atractores como generadores de señales pseudoaleatorias para realizar el proceso de codificación y encriptamiento. El esquema de codificación se basa en una familia de mapas cuadráticos bidimensionales, cuyas salidas presentan comportamiento caótico, con distintos atractores conforme a los coeficientes que se empleen. La idea es que cada palabra a codificar sea unívoca con un juego de coeficientes que serán parámetros de un mapa cuadrático bidimensional. Como resultado de este procedimiento, la señal de salida son puntos pertenecientes a distintos atractores elegidos por la información a transmitir.

La ventaja de este método reside en que la estructura de toda la familia de mapas es única y común, modificándose solamente los coeficientes se consiguen atractores distintos. Esta propiedad reduce y facilita la implementación en hardware. Resultados preliminares obtenidos mediante simulaciones muestran que el sistema presenta una performance comparable a la obtenida en sistemas clásicos de encriptamiento, en cuanto a probabilidad de error y a distancia mínima.

2.1.2. Mapas cuadráticos bidimensionales

En este trabajo se emplea una familia de mapas cuadráticos bidimensionales cuya estructura consta de dos ecuaciones cuadráticas en diferencias acopladas (Ec.2.1). La característica principal de este mapa es que los parámetros, a_i y b_i , son coeficientes reales y para ciertos valores de estos coeficientes la salida del sistema presentará comportamiento caótico.

Se obtiene así un subgrupo de mapas distintos con comportamiento caótico según la elección de estos coeficientes, en la Fig. 3.1 puede verse tres atractores para tres juegos distintos de valores de los coeficientes.

Estos mapas han sido ampliamente estudiados, por lo que la estabilidad, la sensibilidad a las condiciones iniciales y su dimensión fractal son parámetros ya conocidos [?, ?].

$$\begin{aligned}x_{n+1} &= a_0 + a_1 x_n + a_2 x_n^2 + a_3 x_n y_n + a_4 y_n^2 + a_5 y_n \\y_{n+1} &= b_0 + b_1 x_n + b_2 x_n^2 + b_3 x_n y_n + b_4 y_n^2 + b_5 y_n\end{aligned}\quad (2.1)$$

2.1.3. Implementación

Desde el punto de vista del esquema de codificación propuesto, estos mapas son muy atractivos por el hecho de contar con 12 coeficientes para generar cada

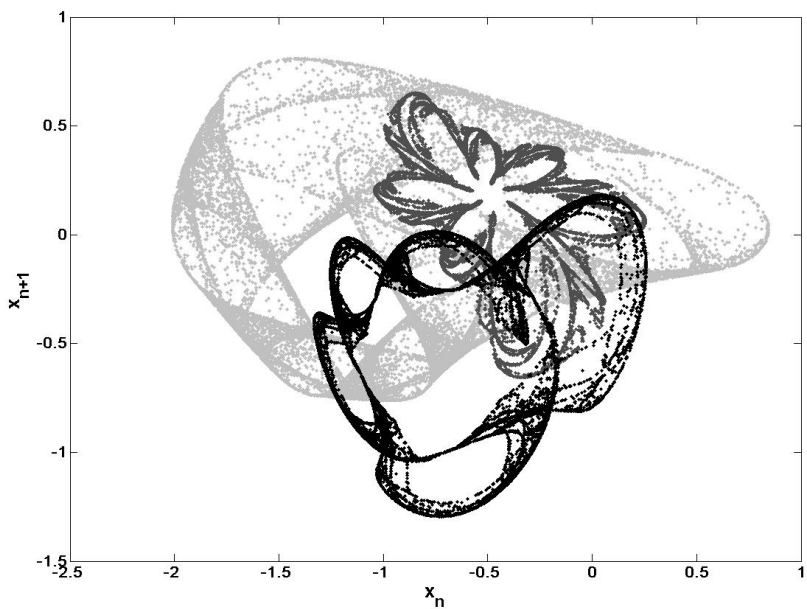


Figura 2.1: Atractores del sistema para tres juegos de coeficientes.

atractor. Por lo tanto, las combinaciones posibles serán N^{12} , en donde N es la cantidad de símblos posibles según la aritmética utilizada. En nuestro caso empleamos una aritmética de 19 bits expresados en complemento a 2 con aritmética de punto fijo, con 1 bit de signo, 3 bits de parte entera y 15 bits de parte decimal. Esta aritmética limita y discretiza el plano xy que queda delimitado por $\Delta x = 4$, $-\Delta x = -4$, $\Delta y = 4$, $-\Delta y = -4$, como puede verse en la figura 3.1. Estas limitaciones al plano de atracción tienen como consecuencia dos cuestiones a tener en cuenta:

- Debido a que los coeficientes se generan con la misma aritmética que las variables, nos encontramos con $N = 2^{19}$ valores posibles para cada coeficiente, lo que arroja $(2^{19})^{12} \cong 4,368$ combinaciones posibles de coeficientes para generar distintos atractores.
- En cuanto a las trayectorias de los atractores sobre el plano discretizado, éstas se tornan periódicas debido a la discretización.

No todos los juegos de coeficientes generan atractores caóticos contenidos en el plano dado por la aritmética utilizada. Aunque esto no sería problema para la codificación/decodificación, se eligieron los coeficientes de modo que se generen atractores contenidos en el plano a modo de validación visual.

Dada la naturaleza de los mapas caóticos, un punto muy lejano a la zona de atracción puede hacer que el punto calculado para la próxima iteración diverja, por lo tanto las condiciones iniciales deben ser normalizadas antes de cambiar al mapa siguiente. Para solucionar este problema se utiliza la siguiente estrategia: Primero se define el plano mínimo que contiene al atractor. Para identificarlo se simularon los mapas mediante Quartus generando secuencias de salida lo suficientemente largas como para verificar la periodicidad. Luego se analizó este vector de datos con Matlab buscando los valores extremos en cada una de las variables: $X_{1\max}$, $X_{1\min}$, $Y_{1\max}$, $Y_{1\min}$. Estos límites delimitan al plano mínimo que contiene al atractor. La normalización dada por la ecuación 2.2 se aplica a la salida (x, y) para mapear este plano mínimo a todo el plano delimitado por la aritmética utilizada de dimensiones Δx , $-\Delta x$, Δy , $-\Delta y$. Segundo, se halla el plano máximo que contiene las condiciones iniciales que hacen que no diverja la solución sinó que genere el atractor. Para esto se realizó un programa en Matlab que genera los atractores desde todas las condiciones iniciales del plano delimitado y discretizado por la aritmética utilizada, a continuación se marcan todos los puntos que generan trayectorias divergentes o bien convergentes a un punto fijo. Este proceso genera la zona de condiciones iniciales factible para generar atractores, nuevamente se identificaron los valores máximos y mínimos del área rectangular máxima que contenga todos sus puntos como condiciones iniciales factibles $X_{2\max}$, $X_{2\min}$, $Y_{2\max}$, $Y_{2\min}$. La normalización dada por la ecuación 2.3 se aplica a la entrada

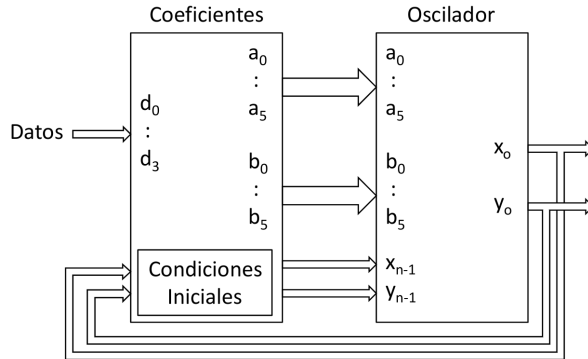


Figura 2.2: Generador de atractores.

de condiciones iniciales (x_{n-1}, y_{n-1}) para mapear todo el plano de dimensiones Δx , $-\Delta x$, Δy y $-\Delta y$ al de condiciones iniciales factibles.

El problema de la existencia de puntos fijos para cierto conjunto de coeficientes y condiciones iniciales queda salvado al perturbar continuamente al atractor actual con valores afectados por la información.

Se generó un circuito en VHDL con un total de 16 juegos de parámetros seleccionables con la palabra de entrada de 4 bits que se desea encriptar. Esta palabra multiplexa estos coeficientes y alimenta un oscilador que calcula la próxima iteración de datos, además, este circuito almacena la salida del oscilador y la realimenta como “condición inicial” para calcular la iteración siguiente (Fig. 2.2). Como resultado de este proceso, la salida encriptada resulta ser el oscilador actual seleccionado por la palabra de entrada perturbado por la historia de los mapas seleccionados por las entradas anteriores. Este circuito de dos bloques se encarga de generar los atractores, por lo que se lo llama “generador de atractores”.

Para la primer iteración, las condiciones iniciales son $(x; y) = (0,1; 0,1)$ para cualquiera de los atractores.

$$\begin{aligned}
 x_{1norm} &= a_{1x}x + b_{1x} \\
 y_{1norm} &= a_{1y}y + b_{1x} \\
 a_{1x} &= \frac{2\Delta x}{x_{1max} - x_{1min}} \\
 a_{1y} &= \frac{2\Delta y}{y_{1max} - y_{1min}} \\
 b_{1x} &= -\frac{x_{1max} - x_{1min}}{2} \\
 b_{1x} &= -\frac{y_{1max} - y_{1min}}{2}
 \end{aligned} \tag{2.2}$$

$$\begin{aligned}
 x_{2norm} &= a_{2x}x + b_{2x} \\
 y_{2norm} &= a_{2y}y + b_{2x} \\
 a_{2x} &= \frac{x_{2max} - x_{2min}}{2\Delta x} \\
 a_{2y} &= \frac{y_{2max} - y_{2min}}{2\Delta y} \\
 b_{2x} &= \frac{x_{2max} - x_{2min}}{2} \\
 b_{2x} &= \frac{y_{2max} - y_{2min}}{2}
 \end{aligned} \tag{2.3}$$

Codificador

El bloque del Codificador consiste en circuito generador y acondicionamiento de la salida. Para codificar una palabra de cuatro bits de entrada se generan los valores de x e y con el circuito generador correspondiente a esta palabra y se los concatena en un circuito posterior formando un vector $[x : y]$ (Fig. 2.3). De esta forma cada palabra de información a ser enviada será representada por la salida xy del oscilador del atractor correspondiente, por lo tanto una palabra a codificar no se corresponderá con una palabra codificada, dos palabras iguales generarán dos salidas distintas.

Decodificador

Un segundo circuito generador de atractores funciona en el decodificador generando las 16 palabras posibles para la próxima iteración. Luego, se ingresan todas estas posibles palabras cifradas junto con la que se desea decodificar a un comparador que aplica una XOR a la palabra ingresada contra todas las palabras

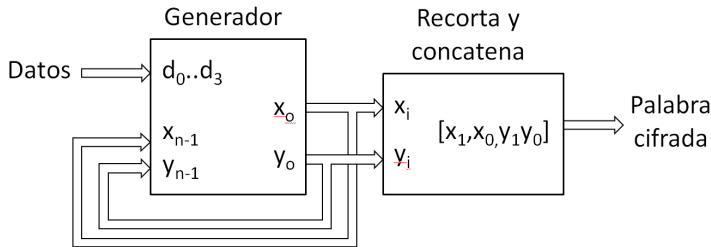


Figura 2.3: Codificador.

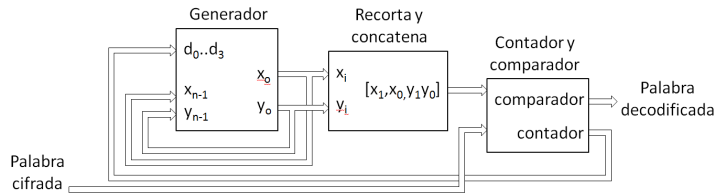


Figura 2.4: Decodificador.

posibles generadas localmente para decodificarla. La salida de este circuito es la palabra decodificada (Fig. 2.4).

2.1.4. Resultados

Se realizó un primer esquema del diseño mediante la herramienta Quartus II v8.0 de ALTERA, para implementar el sistema en una FPGA *Altera Cyclone III EP3C120*

Se obtuvieron resultados preliminares de simulaciones realizadas mediante el programa Matlab y mediante simulaciones con el programa Quartus de Altera, estas últimas tienen en cuenta el empleo de la precisión finita elegida para representar los valores.

En la Fig. 2.5 se pueden ver las salidas del bloque generador para una transmisión de los datos $[1,2,3,2,3,3,1,3,1,3,1]$. En este caso se mantiene el dato a enviar durante 100 ciclos con el objetivo de que sea visible en la figura, en el sistema real cada oscilador codifica una palabra de información en cada iteración. Aquí puede observarse que el sistema cambia el atractor generado según los coeficientes que dependen de la entrada de información a transmitir.

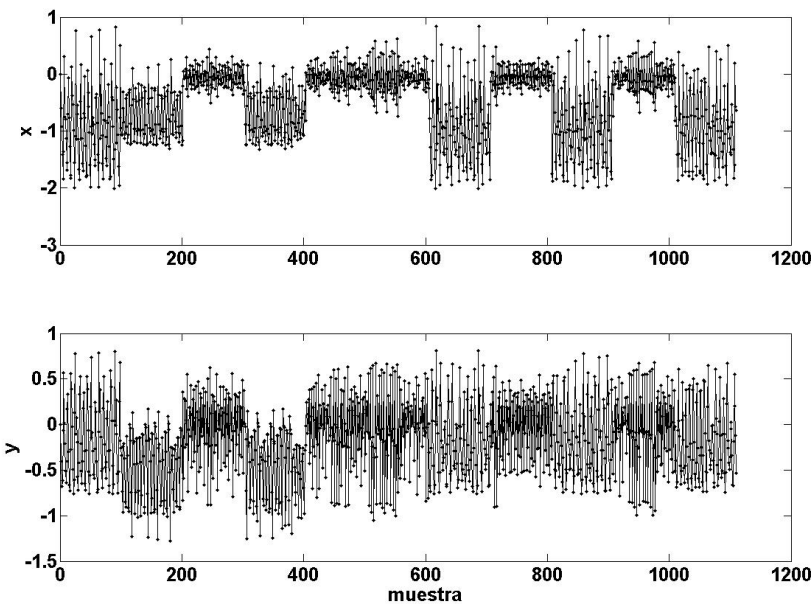


Figura 2.5: Señales a transmitir.

En cuanto al análisis de performance que presenta el sistema se deben tener en cuenta dos aspectos:

- La distancia mínima de la modulación codificada resultante. Esta es usualmente empleada para proveer un límite de error en la región de piso.
- Una descripción precisa de la tasa binaria de error del sistema o BER (en inglés, Bit Error Rate) también es un parámetro muy importante, ya que da una estimación del comportamiento que presentara el código.

2.2. Codificación variable en el tiempo empleando mapa caótico (póster CASE2012)

Los posters no se si agregarlos o distribuir la información entre los demás capítulos.

2.3. ESTUDIO DEL CAOS EN REDES NEURONALES DISCRETAS PARA SU IMPLEMENTACIÓN EN HARDWARE

En el diseño de un sistema de comunicaciones de datos inalámbrico tanto la confiabilidad de la transmisión como el nivel de privacidad son objetivos a cumplir. Han surgido últimamente técnicas de codificación que permiten además de aumentar la confiabilidad de la transmisión frente al ruido adicionar al sistema algún nivel de seguridad. En este trabajo se propone un esquema de codificación que cumple con ambos objetivos. Este sistema se basa en un mapa cuadrático bidimensional cuya salida presenta un comportamiento caótico y distintos atractores dependiendo de los coeficientes que se empleen. Codificar significa básicamente tomar las 2^k palabras binarias de k bits que se pretende codificar, y asignarlas a algunos de los 2^n vectores de n bits. Esto se realiza como una función unívoca entre los 2^k y los 2^n vectores. Siendo regularmente $k \leq n$ existen más vectores de n bits que los que se tienen de k bits. Tradicionalmente el subgrupo de 2^n palabras código es fijo y la elección de los vectores de n bits se realiza empleando la menor redundancia, y maximizando la distancia o separación entre las palabras. En este trabajo la asignación de los vectores es variable ya que a cada una de las 2^k palabras a transmitir se le asigna un juego de coeficientes que genera salida caótica del mapa. Según la palabra a transmitir el sistema generará una salida determinada por los coeficientes y el valor inicial, esta será la palabra código correspondiente a la palabra a enviar. De esta forma, el subespacio de palabras código va cambiando a medida que la transmisión evoluciona.

2.3. Estudio del Caos en Redes Neuronales Discretas para su Implementación en Hardware (Informe Inteligencia computacional, Poster CASE2014)

Este es bastante largo y completo, pero perdí todos los archivos junto con el disco, tengo el pdf a partir del cual voy a tener que armar el latex de nuevo.

Dentro de los sistemas complejos se encuentran los cónicos, éstos se caracterizan por tener propiedades estocásticas similares a los de los sistemas aleatorios (en algunos casos mejores), por ser muy sensibles a las condiciones iniciales y por ser impredecibles a mediano plazo a pesar de contar con las ecuaciones que describen el sistema. Numerosos trabajos describen el comportamiento caótico en redes neuronales, este trabajo presenta una detallada descripción técnica de un caso de estudio.

2.4. *RO*-based *PRNG*: *FPGA* implementation and stochastic analysis

2.4.1. Introduction

The jitter and phase noises present in ring oscillators, are not convenient in several applications of *ROs*, for example in the implementation of *on-chip oscillators* to generate clocks in high-speed circuits[?, ?, ?]. However they are the source of randomness for *RO*-based *PRNG* [?, ?]. Furthermore *ROs* can be implemented in a full-digital circuit like Field Programmable Gate Arrays (*FPGAs*) as they basically are just a string of inverters.

In [?], Sunar et al. presented a *PRNG* using stochastic jitter by combining several *ROs*. They required a post processing of the bit stream, based on resilient functions, to mask imperfections in the entropy source and to increase immunity against changes in environmental conditions. The entropy of the bit stream was used to validate the results in [?].

Wold et al. [?] proposed an enhanced version with better random characteristics and without a post processing. They only added an extra D flip-flop at each ring output. The effectiveness of their proposal was tested by means of test suites available in the open literature [?, ?, ?].

In this paper a detailed description of a very compact hardware implementation of the *RO*-based *PRNG* proposed in [?] is done. In order to validate the randomness of the noise sequences generated, two quantifiers derived from the information theory are used. They define a dual entropy plane H_{BP} vs H_{hist} . H_{hist} is a measure of the first characteristic of a *PRNG* pointed in the abstract, the equiprobability among all possible values. H_{BP} is a measure of the second characteristic pointed in the abstract, the independence between consecutive values. This methodology was successful to evaluate randomizing techniques applied to chaos-based *PRNG* [?]. A comparison with other options both physical and algorithmic, proposed in the literature is made showing that, in spite of their simplicity, *RO* are good candidates as *PRNG*.

Organization of the paper is as follows: section ?? describes the hardware implementation of the *ROs* mapped in *FPGA* Cyclone III. Section 2.4.3 shows how the normalized entropies are determined (to keep this paper short we do not detail already published results); 2.4.4 presents the results obtained for different configurations of the same *PRNGs* proposed in [?], and the statistical comparison with other utilized *PPRNGs*. Finally we present our conclusions in Sec. 4.2.5.

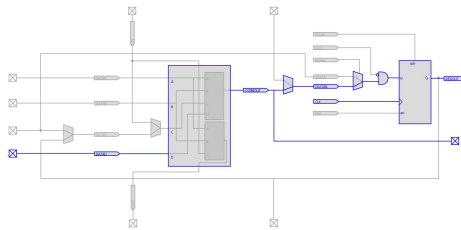


Figura 2.6: *LE* implementing an inverter and a Flip Flop, Chip Planner view.

2.4.2. Hardware implementation.

The implemented *PRNG*'s consist of several *ROs* with their outputs XORed together and sampled by a *D* flip flop. The flip flop latches the output at a selected frequency (here 100MHz)[?]. The physical implementation is made on *ALTERA[©] Cyclone III EP3C120* development kit with a *EP3C120F780C7N* *FPGA*. The design is made with *Quartus[©] II* 13.1 software.

Chip Overview.

FPGAs consist of a large number of logic array blocks (*LABs*), with groups of logic elements (*LEs*) for implementing sequential as well as combinatorial circuits. In the *Cyclone III* family architecture each *LAB* contains 16 *LEs*. Basically, each *LE* is a Flip Flop (*FF*) with a four-input look-up table (*LUT*) (see Fig. 2.6). Each *LUT* can implement any function of four variables. The *FF* and the *LUT* can be used together or independently, [?].

Usually, the logic synthesis software assigns *LE*'s resources without the designer intervention. But in the design of *RO*-based *PRNGs* it is necessary to control the exact location of each individual component for two reasons: 1) to avoid the simplification of the inverters performed by the synthesis tool; 2) to locate each *RO* in the desired place. In *Altera* the use of low-level primitives enables one to control the hardware implementation for each *cone of logic* [?]. Consequently low-level primitives and assignments are employed inside the *HDL* (hardware description language) code employed in our design.

Strings of *ROs* can be programmed on the chip by instantiating the *LUTs* as inverters. In the case of *ROs* it is necessary to prevent the *Quartus II* synthesis engine to merge two *NOT* gates in series, by using a primitive called *LCELL*. A *LCELL* always consumes one logic cell and it is not removed from the project during logic synthesis.

These primitives allow one to break up the design into manageable parts. Each

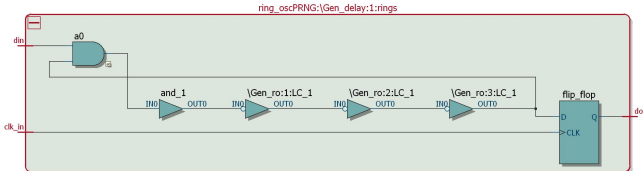


Figura 2.7: RTL view one ring with 3 inverters.

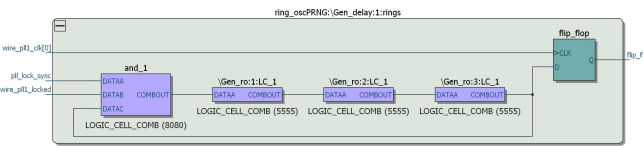


Figura 2.8: Technology map viewer (post mapping), one ring with 3 inverters.

cone is as small as a *LCELL* instantiation. To create a *RO*, *LCELLs* are programmed as inverter-buffers. Figs. 2.7 and 2.8 show how this primitive is implemented by the Quartus II compiler.

Furthermore, to avoid the synthesis tool to optimize removing the redundant buffers away, the Ignore *LCELL* Buffers must be set in *OFF* in the *More Analysis & Synthesis Settings* dialog box. Also *Remove Redundant Logic Cells* must be set to *OFF*.

In order to place each *RO* at a desired position, it must be assigned to a previously defined *LogicLock region*. In this way the *fitter* will keep all the elements of each ring inside the same region, [?]. The process of mapping all the elements to a particular location on the chip (*LogicLock* region) is achieved by the *Assignment Editor* tool, that also allows one to verify that the placements are actually still there, after the *Synthesis* and *Place & Route* processes.

Fig. 2.9 shows the 50 *LogicLock* regions used in this paper as they are established in the die. One *RO* is assigned to each region. Regions are spread over the die for a future analysis of location importance. Each region has 16 *LABs*, to allow us to increase the number of inverters of each ring, an issue to be considered in future work.

3-inverters, employed in a *RO* and the *FF* were all mapped onto a *LE* each, meaning that the block utilization is 4 of 16 *LEs* for any *LAB*.

Fig. 2.6 displays a single *LE*, there an inverter is implemented in the *LUT* and it can be seen the exact *LUT* input that is used. Also the output *FF* of the ring

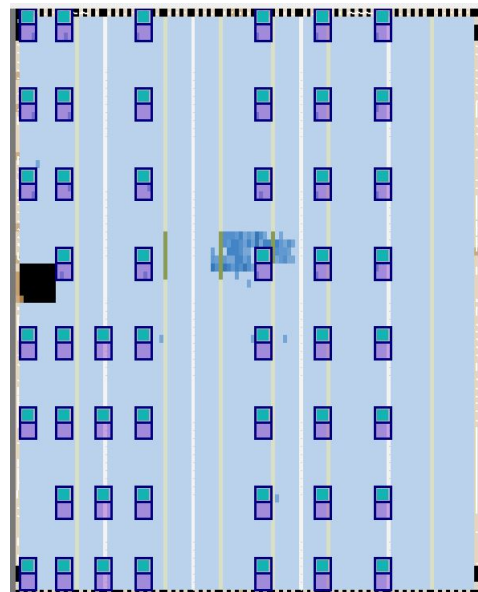


Figura 2.9: *Chip Planner* view *LogicLock* regions.

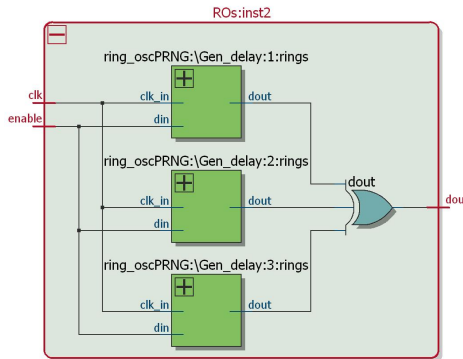


Figura 2.10: *RTL* view of *PRNG* with 3 *ROs*.

is mapped there.

There are many factors that determine the frequency of each *RO*, and contributes to the unpredictability of the output:

1. Placement within the *LAB*: different placements between rings could result in timing differences.
2. Connections: even having exactly identical placement of the *LUTs* with respect to each other in a given ring, it is not possible to have exactly the same *routing resource usage* in the connections. A small difference in *routing resource usage* could affect the ring delay.
3. Input selection: the *fitter* will choose which *LUT* input is utilized during the routing stage. But the delay through the *LUT* depends on which of the four inputs is used and consequently the rings could also have different delays.
4. Neighborhood: even if the design locks down all the placement and routing of a section and everything is physically locked, the timing can change by a few picoseconds depending on what is placed and routed around the ring.

In Fig. 2.10 (RTL view) it is shown a *PRNG* using 3 *ROs* followed by a XOR gate.

Finally, Table 2.1 shows the compilation report of the *PRNG* using 15 *ROs* each with 3 inverters.

Total logic elements	847/119,088	(< 1 %)
Total combinational functions	629/119,088	(< 1 %)
Dedicated logic registers	617/119,088	(< 1 %)
Total registers	617	
Total memory bits	131,072/3,981,312	(3 %)

Cuadro 2.1: Compilation Report, *RO*-based *PRNG* using 15 *ROs* and 3 inverters each.

2.4.3. Quantifiers

Let $X = \{x_i, i = 1, \dots, N\}$ be a length N output of a given symbolic source with alphabet $\mathcal{A} = \{a_i, i = 1, \dots, M\}$. Each element of X is $x_i \in \mathcal{A}$. In the case of *RO* the alphabet is binary consisting of two symbols $\mathcal{A} = \{0, 1\}$. The output is converted into words of n elements. In our case $n = 6$. It means we work with a time series $Y = \{y_i, i = 1, \dots, K\}$ with $K = N/6$ of natural numbers $y_i \in [0, 2^6 - 1]$.

The obvious *PDF* (probability density function) to characterize Y is the normalized histogram of the K words Y ; let us call it PDF_{hist} . Its normalized Shannon entropy H_{hist} is given by:

$$H_{hist} = \frac{\sum_{i=1}^K p_i \log p_i}{\log K} \quad (2.4)$$

We call this *PDF non-causal* because it does not change if we permute the time order of the words, and consequently can not detect any causal connection between consecutive words. The normalized entropy H_{hist} quantifies the equiprobability of the words among all possible values. For a *PRNG* its ideal value is $H_{hist} = 1$.

To quantify statistical independence between consecutive words we use a *causal PDF*, proposed by Bandt & Pompe [?]. This *PDF* is obtained by assigning ordering patterns to overlapped segments, of length D , of the time series trajectory. The process is as follows: 1) group D consecutive words $\{y_i, y_{i+1}, \dots, y_{i+D}\}$ (let us stress that in our case each y_i is a natural number $\in [0, 63]$). The ordering of the D values inside each group is compared with the order of numbers $\{1, 2, \dots, D\}$. There exist $D!$ possible permutations of D elements. Each permutation is called an *ordering pattern* [?] and is labelled with a permutation number $\pi = 1, \dots, D!$. The normalized histogram of π_i 's is called the Bandt & Pompe *PDF*, PDF_{BP} . The normalized Shannon entropy of this PDF_{BP} is H_{BP} where the subscript *BP* means “Bandt and Pompe”.

In case two values of y_i inside the same group are identical, it is considered that the first one is lower than the last one in order to obtain an unique result. For *PRNGs* this procedure does not produce significant changes in PDF_{BP} .

The Bandt & Pompe procedure has the advantages of being: 1) simpler and fast to calculate than block entropies, 2) robust in presence of noise, and 3) invariant to lineal monotonous transformations. It is applicable not only to *PRNGs* but also to any weak stationary process (it means for $k = D$, the probability that $x_t < x_{t+k}$ does not depend on the particular t [?]). The causality property of PDF_{BP} makes the quantifiers based on this PDF to discriminate between deterministic and stochastic systems [?].

Bandt and Pompe suggested $3 \leq D \leq 7$. $D = 6$ is adopted in this work.

A full discussion about the convenience of using different quantifiers to measure a given PDF 's is out of the scope of this work. Nevertheless reliable bibliographic sources do exist [?, ?, ?, ?, ?, ?, ?, ?].

In this paper we adopt plane H_{BP} vs H_{hist} [?] to represent each *PRNG*. A higher value in any of the entropies, H_{BP} and H_{hist} , implies an increase in the uniformity of the involved PDF 's. The point (1, 1) represents the ideal point for a *PRNG* with uniform histogram and uniform distribution of ordering patterns.

2.4.4. Results

The *Embedded Logic Analyzer* tool is utilized for collecting the random sequences generated. It constitutes a *system-level debugging tool*, provided by *Altera* [?], that captures and storages the real-time signal behavior and allows one to observe interactions between hardware and software in system designs. After acquiring the data and save them into a *SignalTap II* file, they can be analyzed or viewed as a waveform. With this procedure nor extra jitter neither distortion are introduced in the measured signal from the data acquisition chain.

In the case of *RO* based *PRNG* data files with 917504 bits each were generated for each *RO* based *PRNG*. We consider sets of N_{RO} rings, each with 3 inverters; $N_{RO} = 2, 3, 4, 5, 6, 7, 15, 25$ and 50.

Data from *SignalTap* were processed using *Matlab*[©]. Binary data were grouped in 6-bits words without superposition, so files with 152917 data each were generated. Quantifiers described in section 2.4.3 were calculated for all generated files.

We also evaluated other known noises generators to compare their quality with that of the *RO*-based *PRNG*. The noises analyzed are:

- Mersenne Twister pseudo-random number generator, [?].
- Two algorithms employed for generate random data by Matlab (Multiplicative Congruential method) [?] and Excel [?].
- Two *physical noises*: radioactive decay noise [?] and atmospheric noise [?]. Data files for these noises are available from the referred *websites*.

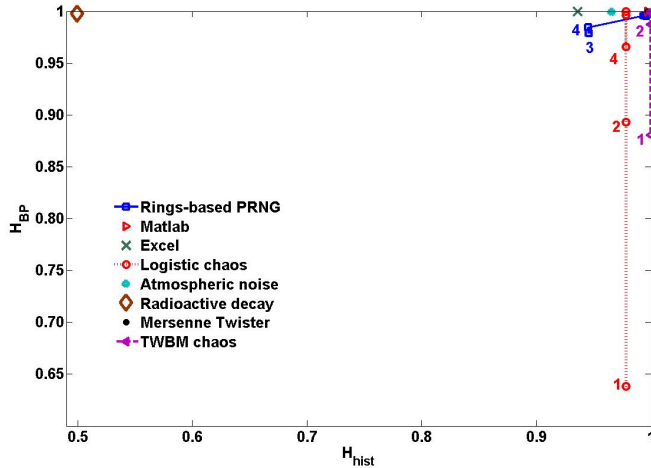


Figura 2.11: H_{BP} vs H_{hist} plane for several noises, numbers next to each square indicate the quantity of ROs used in the RO based PRNG. Numbers next to each point in the chaotic sequences labeled *Logistic* and *TWBM* indicate the number of iteration of the chaotic map (see the text for details).

- Two chaotic map M^1 and their iterated versions M^2 to M^8 [?] for the logistic map (*LOGISTIC*) and the *three way Bernoulli map* (*TWBM*).

Fig. 2.11 shows the results in the dual entropy plane H_{BP} vs H_{hist} for all these noises. It can be seen that the *physical noises*, the algorithmic *Mersenne Twister*, and the *PRNGs* used in *Matlab* [®](*rand* function) and *Excel* [®](*RAND* function), have the maximum value for H_{BP} , indicating that all the ordering patterns appear almost the same number of times. However these five noises present very different behavior with respect the H_{hist} quantifier. The *radioactive decay* is the worst, with a value of H_{hist} about 0,5 indicating that this sequence does not exhibit all possible values in the same proportion. In Fig. 2.11 the numbers next to each marker for the chaotic sequences, indicate the number of iteration. The iterated maps have higher H_{BP} because of their mixing property [?].

In the case of the RO-based PRNG sequences, numbers next to each square indicate the quantity of ROs employed in that PRNG (let us stress that the number of inverters is fixed to 3). The dual entropy plane shows that an increase in the number of ROs improves both H_{BP} and H_{hist} .

Fig. 2.12 is a zoom of Fig. 2.11 around the ideal point (1, 1).

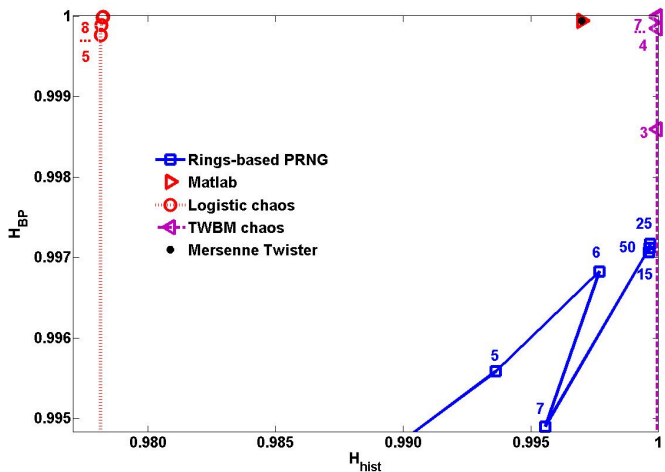


Figura 2.12: Zoom of Fig. 2.11 around the ideal point $(1, 1)$ of the H_{BP} vs H_{hist} plane. Numbers next to each square indicate the number of ROs used in that rings-based PRNG. Numbers next to each point in the chaotic sequences indicate the number of iteration of the chaotic map.

2.5. IMPLEMENTACIÓN DE ALGORITMO GENÉTICO PARA LA BÚSQUEDA AUTOMÁTICA

There, it is shown the evolution of the *RO*-based *PRNG* sequences when the quantity of *ROs* increases from 5 to 50 (numbers next to each square). It can be seen that as the number of rings increases, data increase their mixture and also the histogram tends to be more uniform. So both properties are improved. Here a threshold in the number of rings can be determined, as the points saturate at about (0,997, 1), so this is the best *PRNG* possible. Further, using more than 15 *ROs* presents no improvement. As it was previously said, H_{hist} quantifier detects the histogram variation of the sequence, and the H_{BP} quantifier reflects the improvement in the mixing of data. Finally, Mersenne Twister and Matlab sequences present identical value, ideal H_{BP} , and a high value of H_{hist} nonetheless the histogram is not perfectly uniform (values are not equiprobable).

2.4.5. Conclusions

RO-based *PRNG* implemented here has demonstrated to satisfactorily meet the statistical properties desired by a *PRNG*. They are comparable of other used *PRNGs* and in some cases they are better. They employs few resources of the device and they are simply to implement in a digital platform.

It was demonstrated that for these architectures of *PRNG* the quantity of *ROs* establishes *PRNG*'s statistical properties. It was seen that for 15 *ROs* both output's statistical properties, histogram and mixing, were almost ideal, making unnecessary the increase of the number of rings.

The dual entropy plane proposed here has demonstrated to satisfactorily discern between the *PRNG*'s two main desired properties, the equiprobability among all possible values and the statistical independence between consecutive values. Thus, it allows to clearly see what needs to be improved in a given sequence.

2.5. Implementación de algoritmo genético para la búsqueda automática de caos en sistemas multiatractores (póster CASE2013)

Se generó una lógica basada en algoritmos genéticos encargada de evolucionar los parámetros del sistema de modo que cada generación tenga un comportamiento caótico mejor que la anterior [3]. El target (fitness function), por lo tanto, es el MLE. Para mayor claridad se separó el diagrama de flujo en dos partes, un diagrama principal y una subrutina. El sistema se inicializa en un conjunto de coeficientes llamado población inicial, semilla o padre y se calcula su fitness function (F_p). Luego, se genera un incremento de estos parámetros generando un hijo, que ingresa a la subrutina Evolution que lo devuelve evolucionado y calcula

su fitness function (F_c) para compararla con la de sus padres. Las posibilidades son tres: el hijo es un parente de la siguiente generación reemplazando al parente o no, o el hijo es descartado. La subrutina Evolution es un algoritmo muy simple basado en mutaciones. Se varían ligeramente los coeficientes del sistema (generando mutaciones) evaluando su fitness function (F_m) buscando un máximo local.

Capítulo 3

Cuantificadores de Aleatoriedad

3.1. Implementación de algoritmo genético para la búsqueda automática de caos (Póster CA-SE 2013)

Se generó una lógica basada en algoritmos genéticos encargada de evolucionar los parámetros del sistema de modo que cada generación tenga un comportamiento caótico mejor que la anterior [3]. El target (fitness function), por lo tanto, es el MLE. Para mayor claridad se separó el diagrama de flujo en dos partes, un diagrama principal y una subrutina. El sistema se inicializa en un conjunto de coeficientes llamado población inicial, semilla o padre y se calcula su fitness function (F_p). Luego, se genera un incremento de estos parámetros generando un hijo, que ingresa a la subrutina Evolution que lo devuelve evolucionado y calcula su fitness function (F_c) para compararla con la de sus padres. Las posibilidades son tres: el hijo es un parente de la siguiente generación reemplazando al parente o no, o el hijo es descartado. La subrutina Evolution es un algoritmo muy simple basado en mutaciones. Se varían ligeramente los coeficientes del sistema (generando mutaciones) evaluando su fitness function (F_m) buscando un máximo local.

3.2. Hardware Implementation of Maximum Lyapunov Exponent

3.2.1. Introduction

The maximum Lyapunov Exponent characterizes how fast two trajectories drift apart, if this rate is exponential the system is said to be chaotic, because of this it is known as a detector of “chaoticity”, [?, ?, ?]. Lately, the *MLE* has been used in many applications, in very different areas. Just to mention a few of them in [?] the Lyapunov exponent is used to judge the chaotic characteristic of gas weak signal as the criteria for chaos, in [?] they studied whether changes in probability of falling of a simple model of human walking (a so-called dynamic walker) could be predicted from *MLE*, in [?] the author use the Lyapunov exponents to predict capsizel events for both intact and damaged stability cases.

It becomes important to have a hardware implementation of a quantifier that calculates the *MLE*. This work is part of a larger and more complex project in which maximum Lyapunov exponent of the data generated by a multiatractor non-linear system is employed in order to increment the level of “chaoticity” of the system.

Multiatractor chaotic systems are a type of dynamics systems with the peculiarity that their attractors critically depend on the values of their parameters, [?, ?]. This becomes particularly risky when digital implementation is performed, because the selection of the quantity of bits employed to represent the system could entirely change the dynamics of it. There are many quantifiers that detect this variations, depending on which property is desired to be monitored. One of them is the *MLE*.

This paper describes a design and hardware implementation of a quantifier that calculates the maximum Lyapunov exponent of a system, employing floating point arithmetic.

3.2.2. Maximum Lyapunov exponent

The Lyapunov exponents are quantifiers that characterize how the separation between two trajectories evolves, [?]. It is generally well known that chaotic behaviors are characterized mainly by Lyapunov numbers of the dynamic systems. If one or more Lyapunov numbers are greater than zero, then the system behaves chaotically, otherwise, the system is stable. In this paper, we employ the maximum Lyapunov number instead of each Lyapunov number as it is one of the most useful indicators of chaos.

The distance between trajectories changes in 2^{MLE} for each iteration, on average. If $MLE < 0$ the trajectories approaches, this may be due to a fixed point,

if $MLE = 0$ the trajectories keep their distance, this may be due to a limit cycle, if $MLE > 0$, the distance between trajectories is growing, and is an indicator of chaos. [?]

There is a non-analytical way to measure it if only the inputs and outputs of the system are accessible. The procedure is the following: the system must be started from two neighbor points in the phase plane, lets call them (x_a, y_a) and (x_b, y_b) , as the system is iterated the Euclidean distance between the two trajectories is measured (d_n in the n_{th} sample) (eq. 3.1), and the b trajectory is relocalized on each iteration (eq. 3.3), obtaining the points (x_{br}, y_{br}) to feed the system. Then the Lyapunov exponent can be calculated as shown in eq. (3.2). The process can be seen in Fig. 3.3.

$$\begin{aligned} d_{0(i-1)} &= \sqrt{(x_{a(i-1)} - x_{br(i-1)})^2 + (y_{a(i-1)} - y_{br(i-1)})^2} \\ d_{1(i)} &= \sqrt{(x_{a(i)} - x_{b(i)})^2 + (y_{a(i)} - y_{b(i)})^2} \end{aligned} \quad (3.1)$$

$$MLE = \frac{1}{n} \sum_{i=2}^n \log_2 \frac{d_{1(i)}}{d_{0(i-1)}} \quad (3.2)$$

$$\begin{aligned} x_{br(i)} &= x_{a(i)} + (x_{b(i)} - x_{a(i)})d_{0(i-1)}/d_{1(i)} \\ y_{br(i)} &= y_{a(i)} + (y_{b(i)} - y_{a(i)})d_{0(i-1)}/d_{1(i)} \end{aligned} \quad (3.3)$$

3.2.3. Chaotic System analyzed

In this case the system under analysis is a family of bi-dimensional quadratic maps whose structure consists of a pair of coupled quadratic difference equations (eq. 3.4). Each set of parameters a_n and b_n , produces a different evolution of the system. This characteristic is called *multiattractor*, and means that the chaotic behavior of the system changes with the parameters selection, in Fig. 3.1 can be seen three different attractors corresponding to three different sets of parameters.

$$\begin{aligned} x_{(i+1)} &= a_0 + a_1 x_{(i)} + a_2 x_{(i)}^2 + a_3 x_{(i)} y_{(i)} + a_4 y_{(i)}^2 + a_5 y_{(i)} \\ y_{(i+1)} &= b_0 + b_1 x_{(i)} + b_2 x_{(i)}^2 + b_3 x_{(i)} y_{(i)} + b_4 y_{(i)}^2 + b_5 y_{(i)} \end{aligned} \quad (3.4)$$

In [?], the chaotic generator is explained in detail. In order to be embedded in this design, the arithmetic employed there had to be changed, switched to the IEE754 32-bits floating point standard used here.

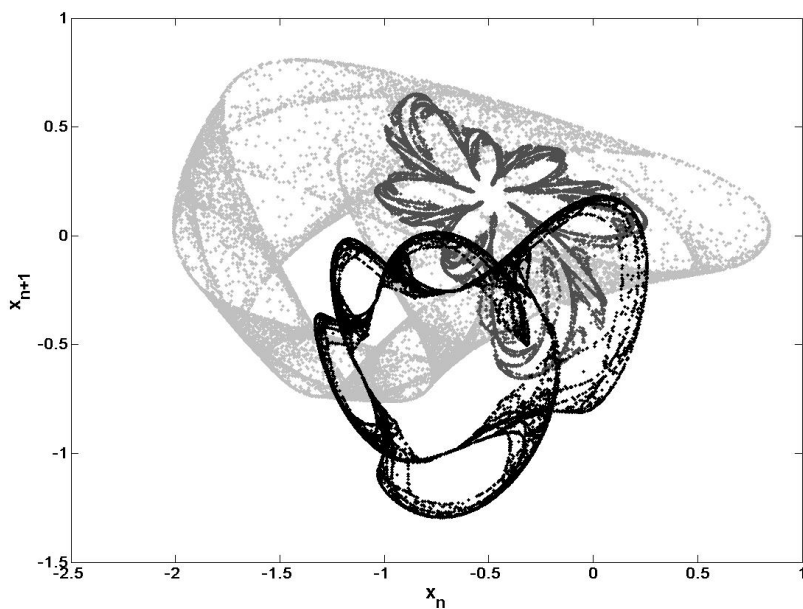


Figura 3.1: Three attractors for three different values for coefficients a_n and b_n .

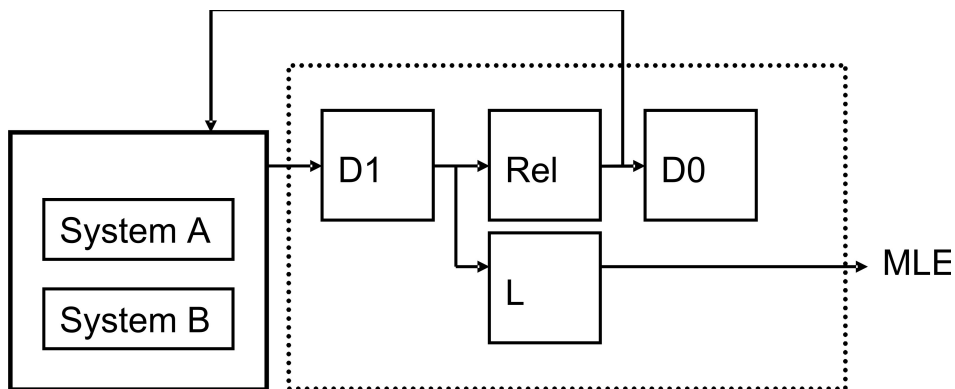


Figura 3.2: Enabling flow of the System.

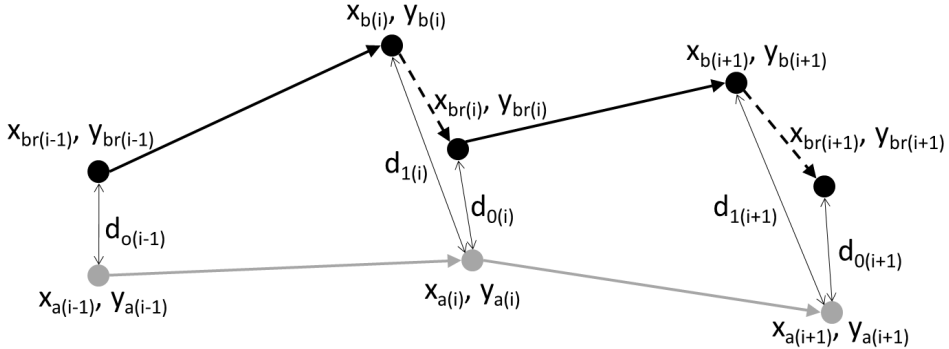


Figura 3.3: Algorithm for calculating the Maximum Lyapunov exponent.

3.2.4. Design of the System

In Fig. 3.2 a block diagram of the enabling flow can be seen. The system consists of four main blocks and is connected to the chaotic system under test by a wishbone interface. This makes the system independent of the quantifier and allows to easily change the system being tested.

The system is duplicated in two blocks, *SystemA* and *SystemB*, each of them is initialized with points $(x_{a(i-1)}, y_{a(i-1)})$ and $(x_{br(i-1)}, y_{br(i-1)})$ respectively, as explained before. When the chaotic systems finish calculating the outputs, signal *habilita* goes to zero and block D_1 is enabled to calculate the Euclidean distance of those outputs, $(x_{a(i)}, y_{a(i)})$ and $(x_{br(i)}, y_{br(i)})$. Then, concurrent blocks L and *Rel* are enabled. The relocated points to feed *SystemB* are calculated by *Rel* block. *Rel* block only needs the current value of d_1 and the previous value of d_0 , as shown in eq. 3.3. When $x_{br(i)}$ and $y_{br(i)}$ are available, *System*'s blocks are enabled to continue calculating and get the next iteration, also block D_0 is enabled to calculate the current value of $d_{0(i)}$ that will be employed in the next iteration.

Finally, L block is in charge of performing the division of d_0 and d_1 , then calculating the absolute value and logarithmic of it. Before that it makes the addition of the $N = 250000$ outputs and divide them by N .

Each block was implemented using VHD language and also IP cores provided by ALTERA (megafunctions, [?]) whenever was possible, because this cores are optimized for this device. Floating point operations such as sums, multiplications, absolute values, logarithms were all calculated with the megafunctions provided by ALTERA.

The working frequency of each block is *clk* and is provided by the *PLL* in order to not to overcome the maximum frequency allowed given by the Altera Timing Analyzer, [?].

In Fig. 3.4 the hole system can be seen in Block Diagram/Schematic file of Quartus environment. There, block *CTReset* is a VHDL file that filters the rebound of the power-on switch. It enables a PLL that decreases the operation frequency, in order to meet the TimeQuest Timing Analyzer requirements. When this PLL locks the frequency it turns down *reset* signal and the systems starts. As predicted by Fig. 3.2 blocks *Rel* (called *Relocalizador* in Fig. 3.4) and *L* are concurrent. The four blocks are designed in the same way, an example is shown in Fig. 3.5 where it is shown the implementation of *D1* block. The inputs, points *a* and *b*, are taken each time signal *habilita* goes down. Then, the signals are processed according to eq. 3.1 employing Floating Point Altera Megafunctions [?] to calculate the Euclidean distance d_1 . Internally, blocks *Rel*, *L* and *D0* are the same as block *D1*, the only differences are the operations they perform accordin to eqs. 3.3, 3.2 and 3.1 respectively. These operations are performed at the maximum frequency *clk*. Outputs of block *L* are for testing purposes, the final design will just keep *L_sal* output.

3.2.5. Results

The system is synthesized and experimentally verified on the Altera CYCLO-NE III FPGA and the results are shown in Fig. 3.8. The Timing Analysis reports that the frequency must be at the most 84,95MHz, so the clock of the board (125MHz) had to be divided to solve this limitation. A PLL provided by Altera, *ALTPPLL* [?], was employed to divide the frequency of the board by 2 (*reloj* block of Fig. 3.4).

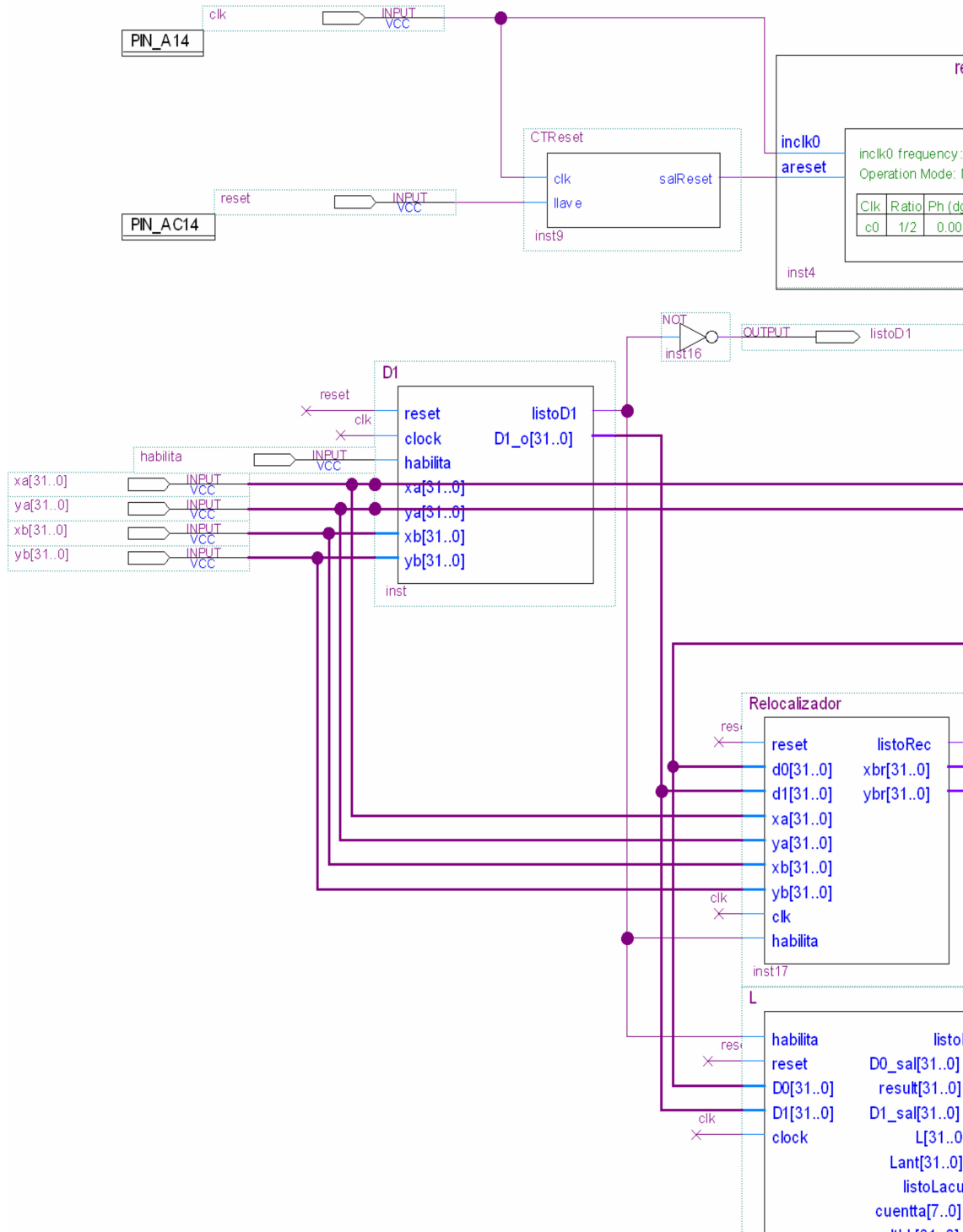
The Compilation Report (Fig. 3.8) shows that the logic utilization does not exceed 25 % this means 29307 total logic elements. 54 % of the total memory bits and 8 % of the 9-bit embedded multiplier.

In Figure 3.6 the Signal Tap output can be seen. There, three signals are shown: the one called *salida* is the sum of *MLE* on each iteration (eq. 3.2). The second signal, called *cuenta_sal* corresponds to the number of the current sum. Finally, each falling edge of the signal *listoD1* indicates that the output is valid. The output is expressed in IEE754 32-bits floating point standard, so the data was processed with Matlab to obtain the Lyapunov curve seen in Fig. 3.7. The value of *MLE* at sample 250000 is 0,1415 and it is consistent with the *MLE* obtained using Matlab.

3.2.6. Conclusions

From the results presented herein, it is possible to conclude that the developed quantifier accurately calculates the *MLE* of a system. We exploit the underline parallel nature of the *MLE* computation equations with the aim of optimizing

3.2. HARDWARE IMPLEMENTATION OF MAXIMUM LYAPUNOV EXPONENT 29



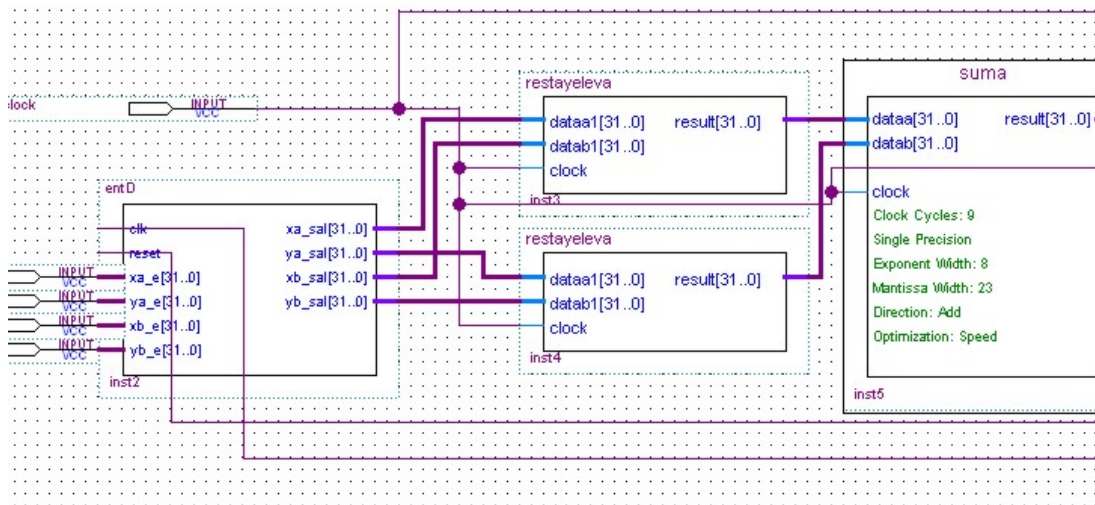
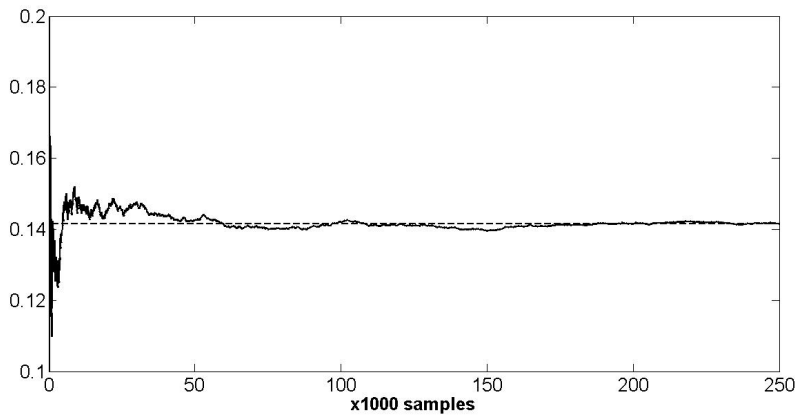


Figura 3.5: D_1 block in Block Diagram/Schematic file of Quartus environment.

Type	Alias	Name	-4085	altr4084	-4096	-3584	-3072	-2560	-2048	-1536	-1024	-512
out		+salida	1171429278		1171430150	1171430139	1171430659	1171431953	1171431895	1171433747	1171	
out		+cuenta_sal	95475	95475	95476	95477	95478	95479	95480	95481	95	
out		listoD1	1									

Figura 3.6: Quartus Signal Tap output.

Figura 3.7: Output of the system *MLE*.

Flow Summary	
Flow Status	Successful - Fri Apr 19 10:20:17 2013
Quartus II 32-bit Version	12.1 Build 177 11/07/2012 SJ Web Edition
Revision Name	CalculaLyap
Top-level Entity Name	TOP
Family	Cyclone III
Device	EP3C120F780C7
Timing Models	Final
Total logic elements	29,307 / 119,088 (25 %)
Total combinational functions	26,048 / 119,088 (22 %)
Dedicated logic registers	18,014 / 119,088 (15 %)
Total registers	18014
Total pins	197 / 532 (37 %)
Total virtual pins	0
Total memory bits	2,133,356 / 3,981,312 (54 %)
Embedded Multiplier 9-bit elements	48 / 576 (8 %)
Total PLLs	1 / 4 (25 %)

Figura 3.8: Quartus Compilation report.

the proposed architecture design, allowing its concurrent implementation based on FPGA technology.

3.3. Causal and Non-causal Entropy quantifiers implemented in FPGA

3.3.1. Introduction

In the development of new electronic realizations of NonLinear Systems, specially Multiatractor chaotic Systems it is critical to be able to know and monitor the system's properties. Always a thorough analysis of the systems is required to meet the objectives, mainly the changes in the statistical properties induced by discretization of the system. Then it is necessary to check that the system still satisfies the application's requirements, this demands further analysis. Tools coming from the nonlinear analysis like Lyapunov exponents, cross, and autocorrelation, Perron-Frobenius operator, Correlation Dimension are employed, and also statistical tools like the Shannon Entropy, Complexity, Bandt and Pompe embedding.

This work is part of a more ambitious project, which is the hardware development and implementation of tools for the analysis of nonlinear systems. These tools will mean a significant advance in the field of implementation of nonlinear systems. It will allow to more accurately understand and describe the behavior of the digital version of this type of systems. The complete package of tools that we intend to implement consists of:

- functional of the probability distribution: Shannon Entropy, Statistical Di-sequilibrium, and Statistical Complexity;
- time series's quantifiers, especially Lyapunov exponents, autocorrelation, cross-correlation and fractal dimensions;
- Perron-Frobenius operator, quantifiers of recurrent plots;
- Statistical tests proposed in standardized banks for studying random number generators (Marsaglia, NIST, etc.).

At the moment, there is no much literature on hardware implementations of these tools [?].

In the particular case of entropy, it is used in various applications, such as in the anomaly detection of IP data flows [?, ?]. In [?] an FPGA design and simulation of an entropy quantifier is introduced, however currently there are no available hardware implementations of this quantifier.

Within the project mentioned in this paper a system that calculates the entropy of a particular probability distribution (PDF) associated with a data set is implemented. Causal and non-causal PDFs are analyzed. Data can have a digital source (generated by code) or can come from sampling external analog signals. The development board used the *M1AFS-embedded kit*, based on the *M1AFS1500* chip that is known for having an analog block embedded in the same package of the FPGA.

Then, the numerical accuracy of the implemented quantifier is verified by comparing their results with a standard program. The maximum error detected determines the statistical accuracy of the system.

The organization of this paper is as follows: Section 3.3.2 both normalized entropies are presented for their consideration; Section 3.3.3 describes the hardware implementation and interfaces; in 3.3.4 the software is described in detail; Section 4.2.3 shows the obtained results of the system validation and in the measurement of the signals. In section 3.3.6, experimental results are interpreted and discussed. Finally, we present our conclusions in Section 3.3.7.

3.3.2. Causal and Non causal Entropy

Let $X = \{x_i, i = 1, \dots, N\}$ of length N the output of a given source symbol, with alphabet $\mathcal{A} = \{a_i, i = 1, \dots, M\}$. Each element of X is $x_i \in \mathcal{A}$.

The most commonly used *PDF* is the normalized histogram of the N values of X between the M symbols of \mathcal{A} ; it is defined as $PDF_{hist} = \{p_i, i = 1, \dots, M\}$, where p_i is the probability of occurrence of the symbol $a_i \in \mathcal{A}$. Its normalized Shannon entropy is referred to as H_{hist} and is defined:

$$H_{hist} = \frac{\sum_{i=1}^M p_i \log p_i}{\log M} \quad (3.5)$$

The standard entropy H_{hist} quantifies the distribution of the elements of the series among all possible symbols.

If the source is a Pseudo Random Number Generator (PRNG), then all the symbols of the alphabet should appear the same number of times and its (optimal) value will be $H_{hist} = 1$.

PDF_{hist} is non-causal since it does not consider the temporal order of time series' elements. This fact means that the X vector could be rearranged to generate other vector Y , which would have the same histogram as X , and, therefore identical PDF_{hist} and the same value for H_{hist} .

For quantifying statistical independence between consecutive elements, in this paper the causal PDF proposed by Bandt & Pompe in [?] is used. This PDF is obtained by assigning patterns of order to overlapped segments of length D of the time series.

The process for its calculation is the following: first D consecutive elements are grouped $\{x_i, x_{i+1}, \dots, x_{i+D}\}$. Then the (ascending or descending) order of the D values of each group is compared to the order of the vector $\{1, 2, \dots, D\}$. There are $D!$ Possible ways to sort the numbers $\{1, 2, \dots, D\}$. If two values of x_i within the same group are identical, it is considered that the first is lower, to obtain a unique result. Each permutation is called *ordering pattern*[?].

The normalized histogram of the order patterns is the causal Bandt & Pompe's PDF PDF_{BP} . The normalized Shannon entropy of that PDF_{BP} is H_{BP} where the subscript BP means "Bandt & Pompe".

Bandt and Pompe suggest $3 \leq D \leq 7$. For this work, we adopted $D = 6$.

In the H_{BP} vs. H_{hist} plane [?], a higher value in any of the entropy values implies an increase in the uniformity of the involved PDF . The point $(1, 1)$ represents an ideal case were both distributions, distribution of values and distribution of order patterns, are uniform.

A complete discussion about the convenience of using these quantifiers is beyond the scope of this work. A broad study can be found in [?, ?, ?, ?, ?].

3.3.3. Implemented Hardware

The hardware design was based on ACTEL's configuration on the 8051 microcontroller, and peripheral interfaces. It was developed using the software package *Libero Soc v11.3*[®]. The development board used was *M1AFS-EMBEDDED-KIT* that contains an FPGA *M1AFS1500* and peripherals [?].

The *M1AFS1500* embedded chip contains an analog block consisting of nine addressable adapters of four inputs each, a 32 inputs analog multiplexer and a configurable analog-digital converter.

For handling this block, a system also provided by ACTEL is used. This system is based on an 8051 microcontroller, and it also contains drivers of the peripheral among other things [?, ?].

The developed system can be divided into three main stages as shown in Fig. 3.9: the first phase is the Acquisition, which converts the incoming analog signals into digital words. The next step is the Calculation logic stage, it uses the SRAM to perform calculations and coordinate the interfaces, and the last stage is the Presentation which sends the results to a computer through the USB-to-UART interface.

Acquisition Stage

The analog data to be evaluated is entered into the system by using the voltage input *AV2* of the analog block *Analog Quad 2*. This input is mapped to channel seven of the analog multiplexer, and it was configured with an input voltage of

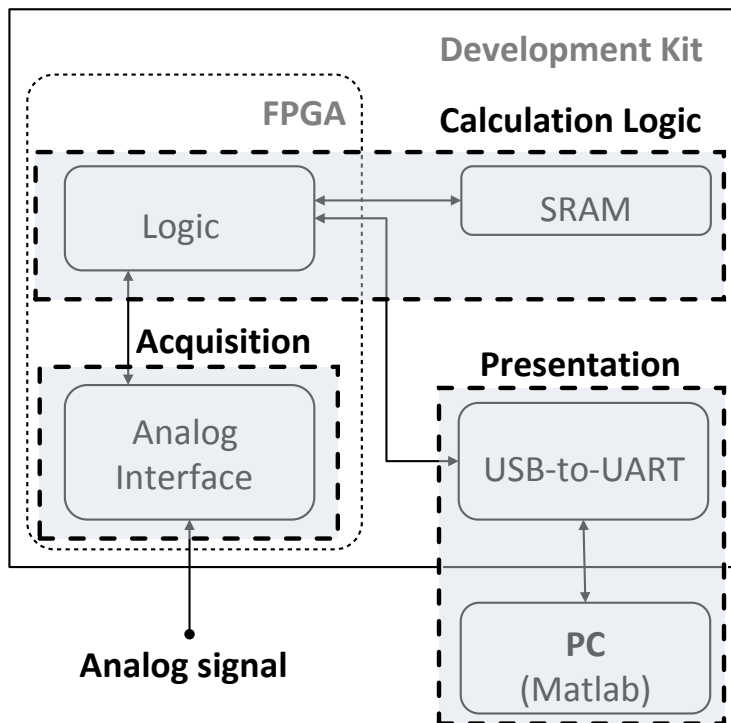


Figura 3.9: Scheme of the complete system.

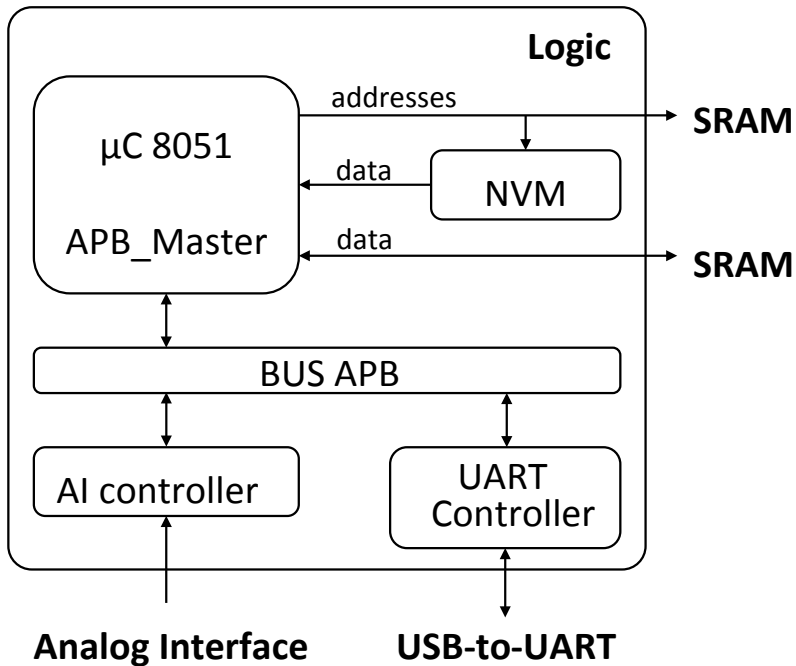


Figura 3.10: Details of the Calculation Logic stage.

0 V to 4 V. The analog-digital converter was configured with a 12-bit resolution. In this first prototype the maximum sample rate achieved was 16 ks/s, limited by the processing logic delay. This speed was enough for the required measurements. However, in a next stage an optimization of the design will be developed by increasing the operating frequency, among other improvements.

Calculation logic

The calculations and synchronization between peripherals are made at this stage. Figure 3.10 shows the main blocks that compose it.

The heart of implementation is an 8051 Core that provides Actel in its library catalog. It is a microcontroller containing the central logic of the Intel 8051 microprocessor, without its peripherals. This micro has a Harvard architecture with a 16 bits address bus, limiting our design to 64 KB of memory code and 64 KB of data memory.

The application that performs the calculations presented in section 3.3.2 runs

over this microcontroller. It is responsible for obtaining the PDFs (BP and hist) and to perform the calculations to get the entropies from the input data, according to Eq. 3.5. Section 3.3.4 describes in detail the developed software. In this particular FPGA, the code memory is a non-volatile memory (NVM) and is implemented in the internal flash of the FPGA blocks. It is mapped onto the addresses from 0x0000 to 0xFFFF and is written during compilation with the contents of a hexadecimal format file.

The system functionality is extended by connecting peripherals through the APB interface.

For handling communication with the PC, the UART controller is used. The output of this block is directed out of the FPGA and is connected to a USB-to-UART chip that is soldered to the board. The analog block is controlled by the AI controller, which routes and synchronizes its inputs.

Presentation

The stage of data presentation involves the USB-to-UART chip adapter that is on the development board and is driven both by the program running on the FPGA as well as by the software that runs on the PC.

The USB-to-UART chip is responsible for adapting the input-output UART logic to an input-output USB standard by which is possible to interact with the PC. Moreover, the program running on the PC handles the user interface and is described in detail in the next section.

3.3.4. Implemented Software

The system operation is achieved by the interaction of two programs. One running on the PC and another on the microcontroller instantiated in the FPGA. It can be seen a flow chart of the two programs and the interaction between them in Fig. 3.11. On the PC runs a Matlab's script that is responsible for opening the serial port where the USB is mapped, requesting data, taking the results of the port, then plotting them in a plane H_{BP} vs. H_{hist} and finally closing the port.

Over the microcontroller instantiated in the FPGA runs a program written in C language and compiled for the 8051 microcontroller using the *SoftConsole IDE v3.4*[©] tool. The firmware used is a modification of [?]. When a request for data from the UART port occurs, the data sampled in the analog input are stored. Then, PDF_{hist} y PDF_{BP} are calculated, and with this information, their respective entropies H_{hist} and H_{BP} are also calculated. These results are sent to the PC through the same port.

To validate the system, and verify how accurate the results are, the incoming sampled vector data is forwarded to the PC, so that it can calculate their entropies

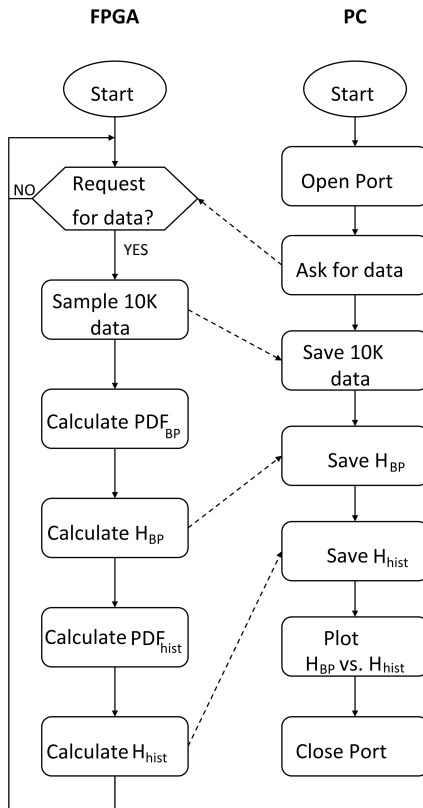


Figura 3.11: Flowchart of the implemented software.

Cuadro 3.1: Quantifiers error evaluated in the FPGA with respect to the results calculated by the pattern program.

Generator	Source	Error H_{BP}	Error H_{hist}
Rand	Digital	$1,7421E^{-6}$	$2,6977E^{-6}$
Logistic	Digital	$0,4256E^{-6}$	$94,693E^{-6}$
Triangular	Analogic	$6,3445E^{-6}$	$2,0028E^{-6}$
Sinusoidal	Analogic	$6,3151E^{-6}$	$5,6506E^{-6}$
Square	Analogic	$0,1797E^{-6}$	$1,9930E^{-6}$
Ramp	Analogic	$245,00E^{-6}$	$1,0876E^{-6}$

with PC using *Matlab*® and compare them with the results of the implemented system.

3.3.5. Results

As said, to test the system, the obtained results were compared with the results achieved by a pattern program running on the PC. For this, 10000 samples of different waveforms were generated by both external (analog) and internal (digital) signals.

Two digital signals were produced by the code in the microcontroller, one corresponds to the rand() C function and the other to the chaotic Logistic map with parameter $r = 4$.

Analog signals were generated with the *HP33120A* waveform generator. With a range of 4 Vpp and 2 V of direct current to take advantage of the full spectrum of the analog-digital converter and increase the signal to noise ratio. In all four cases, the signal frequency was 100 Hz and the sampling rate of 16 ks/s.

Table 3.1 shows the absolute error between the calculated results of the quantifiers in the FPGA compared with the results calculated with the standard program running on the PC, over the same samples.

Fig. 3.12 shows in the H_{BP} vs. H_{hist} plane the results calculated by the FPGA.

Compilation results show the FPGA resources needed by the entire system and also the amount of memory occupied by the software running on the microcontroller. It is important to highlight that this is a rigid hardware implementation, i.e. the first circuit in the FPGA (microcontroller, peripheral, etc.) are configured and then the software is loaded on it. The report returned after running the “Place and Route” tool is shown in Fig. 3.13. It can be seen that the implementation uses 19 % of the FPGA logic resources, 21 % of the input-output cells and 28 % of the memory blocks.

The compilation report of the software part of the system is shown in Fig.

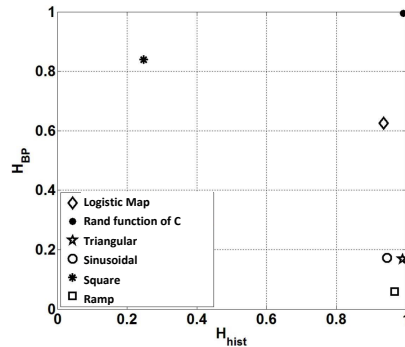


Figura 3.12: Measurement results.

3.14. We can see that the non-volatile flash memory is 15.4 % occupied.

On the other hand, of the 65536 addresses the SRAM have available just 61440 because some of this addresses are used by the APB bus, so the 76,7 % of the available memory is used.

```

Core Cells      : 7349 of 38400 (19%)
IO Cells       : 53 of 252 (21%)

RAM/ROM Usage Summary
Block Rams : 17 of 60 (28%)

```

Figura 3.13: Resources used by the system hardware.

Name	Start	End	Size	Max
PAGED EXT. RAM			0	256
EXTERNAL RAM	0x0000	0xb828	47145	65536
ROM/EPROM/FLASH	0x0000	0x276e	10095	65536

Figura 3.14: Resources used by the system software.

3.3.6. Discussion

The software had to be adapted to the microcontroller instantiated in the FPGAs. The pattern program uses 64-bit floating point arithmetic (IEEE754-64 bits standard) and uses the math.h library [?]. For adapting the algorithm to be able to implement it in the microcontroller that was instantiated in the FPGA, we had

to reduce the number of bits employed. We used 32-bit floating point arithmetic (IEEE754-32 bits standard). The calculation of the logarithm function was also required, so it was implemented using the CORDIC algorithm. These differences make the output of the implemented system not to be equal to that of a program running on the PC, which we take as pattern program. Thus, these differences were measured, to have a dimension and determine whether the results are correct.

Table 3.1 shows that the absolute error never exceeds the value $245E^{-6}$. This boundary indicates that there is a difference from the fifth decimal digit.

It can be seen in Fig. 3.12 that H_{BP} and H_{hist} quantifiers can clearly difference between the statistical properties of the analyzed data. Sinusoidal, Ramp and triangular signals have the highest values for H_{hist} because the present all the possible values that the Analog-digital converter can generate.

However, the mixing of these signals are not good because they are periodic signals, so they are totally predictable, this is reflected by the small values of H_{BP} . An interesting case to be analyzed is the square signal. The additive noise effect is specially marked in the areas where the value of the signal should be constant.

Two very narrow Gaussian curves appear around the ideal values of the PDF_{hist} , this does not affect too much the calculated value of H_{hist} , however for PDF_{BP} , the order pattern is derived directly from the noise, with a particular mean value, so the value of H_{BP} will be higher than expected.

The signal generated by rand function of C has the best statistical properties being located at the point $\sim (1, 1)$.

3.3.7. Conclusions and future work

It was developed and implemented a system that allows a measurement with the proper precision of the causal and non-causal entropy of external analog signals from the outside of the FPGA and internal signals generated by code. It was possible to measure signals and perform complex calculations with a small micro-controller as the 8051 instantiated in ACTEL AFS1500 FPGA. This first prototype meets the required specifications of accuracy and the quantity of resources established in the design. The following step will be to optimize the system regarding operating frequency and noise immunity. It is expected that the system will allow modifying, at runtime, the sampling rate, so it would be adaptable to the input signal, with the upper limit of 500 Ks/s set by the ADC.

A threshold level should be added from which a value will be considered different from another, thus, the problem with the additive noise in the calculation of H_{BP} will be solved. The code for this system occupies 15,4 % of the total flash memory of the instantiated micro, so it will be possible to add software to implement other quantifiers and functionalities. As for the issue of the resources available in the FPGA, the logic cells used is 7349, leaving almost 80 % of the available

hardware resources to implement the systems under test, concurrently with the quantifiers.

3.4. Measuring the Jitter of Ring Oscillators by means of Information Theory Quantifiers

3.4.1. Introduction

Jitter is any light deviation from the mean period of a presumed periodic signal. There are many physical examples where jitter is relevant. Some examples from different areas are: (a) Stalberg et al [?] found that the time interval between the two fibre action potentials of two muscle fibers -belonging to the same motor unit in the normal human muscles- shows a variability or jitter; (b) Mecozzi et al [?] detected timing and amplitude jitter in optical links using highly dispersed pulse transmission; (c) Derickson et al [?] made a comprehensive timing jitter comparison in the case of mode-locked semiconductor lasers; (d) the California and Carnegie Planet Search at Keck Observatory [?] reported jitter in stars radial velocities; (e) Roberts & Guillemin studied the delays due to queueing in upstream multiplexing stages, in an Asynchronous Transfer Mode network (ATM); (f) Baron et al [?] considered the quality of the bunch clock signal of the Large Hadron Collider (LHC), in terms of jitter, a fundamental issue because it synchronizes all the electronics systems in the detector; (g) Marsalek et al analyzed the relationship between synaptic input and spike output jitter in individual neurons [?], etc.

Furthermore, digital instruments are used in any modern experiment and the unavoidable jitter in the data acquisition systems produces uncertainties in time, and consequently in any spectrum determination.

This paper is devoted to Ring Oscillators (*RO*). Let us stress that in this particular application jitter is not always undesirable. Jitter is unwanted in applications that use the *RO* as a clock generator [?, ?, ?, ?, ?]. On the contrary random numbers generators *RNG* using *RO*'s, use jitter as the randomness source, [?, ?]. Jitter also improves the Electromagnetic Compatibility as to distribute the clock frequency over a band, improving the Electromagnetic Compatibility (EMC) [?].

Determination of jitter in *RO*'s has been studied in several papers: in [?] the study of three relevant time domain measures of jitter was presented. In [?] a model for jitter generation and distribution in *RO*'s was proposed. In this seminal paper the authors break up the jitter sources into deterministic and random (gaussian); furthermore each source is additionally classified into local or global. They demonstrate that the most important contributions are the local gaussian jitter and the global deterministic jitter and only the first one must be used as a randomness source of true random number generators (*TRNG*'s). The same ap-

3.4. MEASURING THE JITTER OF RING OSCILLATORS BY MEANS OF INFORMATION TH

proach was used in [?, ?, ?, ?]. Lubicz et al. described a practical and efficient method to estimate the entropy rate of a *TRNG* based on free running oscillators; they emphasized that their method does not require outputting and analyzing the clock signals with external equipment [?] (a methodology that introduces extra jitter and distortion in the measured signal due to the data acquisition chain).

Usually *deterministic jitter* is the name given to any *non-Gaussian jitter*. It is bounded and it is characterized by its peak to peak Δ_{pp} value. Random jitter is the name used for Gaussian jitter and it is unbounded and characterized by its RMS value. Sometimes deterministic periodic jitter appears. It has a *period* that is the interval between two times of maximum (minimum) effect; the inverse of the time period is the *frequency of the jitter*. Periodic jitter with jitter frequency below 10Hz is usually named *wander* and the name *jitter* is reserved only to periodic jitter with frequencies at or above 10Hz. In communications, the *total jitter* is $T = \Delta_{pp} + 2 n R_{rms}$ where n is a number between 6 and 8 related to the Bit Error Rate (*BER*).

RO's are one of the main building blocks in analog and digital integrated circuits and have been extensively used as *on-chip oscillators* to generate clocks in high-speed circuits. Furthermore, *RO*'s can be easily implemented in programmable digital circuits like *FPGAs*. The main advantages of *RO*'s over integrated *LC* oscillators are their smaller chip area, their wider running range (that may be electrically tuned), and their lower power-consumption.

Either one wants to use the *RO* jitter or to eliminate it, jitter must be measured, and it is not a simple task. The main contribution of this paper is to provide a jitter measurement technique based on information theory quantifiers (*ITQ*). We use a stochastic model which randomness is related to the jitter strength. Every proposed *ITQ* used in this paper is based on an entropy, that is a Shannon functional of the probability distribution function (*PDF*) assigned to the time series of the stochastic process. Disequilibrium and complexities may be used as well [?, ?] but they do not represent an improvement in our case. In previous works [?, ?] we showed that many different *PDF*'s can be assigned to the same data string. The best choice depends on the specific application. Two choices for the *PDF* are used in this paper: the *normalized histogram* and the *ordering patterns histogram*. A representation plane is used to compare different situations. Once a *PDF* is chosen, the Shannon Entropy is the basic functional that quantifies the uniformity of the *PDF*. *Normalized entropies*, *differential entropies*, and *rate entropies* are the other *ITQ*'s evaluated. In our case *differential entropies* give the best results and a *differential entropy plane* is used to compare their sensitivity as a jitter measure.

Organization of the paper is as follows: section 3.4.2 describes jitter in *RO*'s and explains how it is measured using random variables; section 3.4.3 details the evaluation of the considered *ITQ*; section 3.4.4 deals with the results using the

proposed quantifiers. Finally, we present our conclusions in sec. 3.4.5.

3.4.2. Determination of jitter in *RO*'s

There are two different situations concerning jitter in *RO*'s: (a) for some applications it is enough to assure that jitter does not perturb the signal over an accepted limit. If this is the case the signal is observed on an oscilloscope with a mask over the display and it is enough to verify that the signal remains within tolerances; (b) in other cases an exact determination of jitter is required. One of these cases is the characterization of *RO*'s, considered in this paper.

Ideal *RO*'s are composed of an odd number of inverters. Each inverter has a propagation time and consequently rising and falling edges separated by half-periods go through the inverters. If all the propagation times are constant the output of this *ideal RO* is a square-wave with a discrete spectrum. But propagation times are not constant as there is jitter. Jitter distorts the delta like power spectrum as each δ is converted into a wider maximum.

Let $T/2$ be the half-period of the *ideal RO*. It is given by:

$$\frac{T}{2} = k \sum_{i=1}^k d_i \quad (3.6)$$

where k is the number of inverters and d_i is the propagation time through the i -th inverter. When jitter exists, d_i are random variables that can be modeled as:

$$d_i = D_i + \Delta d_i \quad (3.7)$$

where D_i is the mean value of d_i with nominal source voltage level and normal temperature, and Δd_i is the delay variation produced by both local physical events and global changes in the device working conditions (as VCC, temperature, etc.). Then jitter in *RO*'s is evidenced by the random displacement of the trailing (falling) edges from their otherwise perfectly periodic location. The direct measurement of this displacement has two main problems: (a) requires a very high-frequency instrument, because time resolution is limited by the sampling period T_s ; (b) this technique introduces extra jitter and distortions in the measured signal coming from the data acquisition chain. Then it is more convenient to use *indirect measurements*, by means of auxiliary random variables related to statistical properties related with jitter to measure jitter with minimal disturbance [?]. The general procedure is as follow:

1. Sample the output with sampling period T_s to get a binary time series. In the ideal case of *no-jitter* the output is a *continuous and perfectly periodic square wave* with period T . Then it is possible to adjust T_s to make $T/2 = m T_s$

3.4. MEASURING THE JITTER OF RING OSCILLATORS BY MEANS OF INFORMATION THEORIES

with $m \in N^+$. The binary time series will be periodic with m 1's followed by m 0's. When jitter is present the binary series is not periodic but stochastic. This stochastic model is known as *alternating renewal process*.

2. Many different randomness quantifiers may be used to characterize the stochastic model associated with the measured jitter. In this paper, we propose the use of *ITQ*'s.

Note that jitter is accumulative and two basic situations arise: (a) if the jitter introduced by each stage is assumed to be totally independent of the jitter introduced by other stages, it means $\sigma_T^2 = m * \sigma_s^2$, where σ_s is the jitter of each sample, and it is supposed that all samples have jitter with the same normal distribution; (b) if jitter sources are totally correlated with one another then $\sigma_T = m * \sigma_s$.

3.4.3. Information Theory Quantifiers

Time series and probability distribution functions

Shannon Entropy is the functional of P more frequently used in the literature (there are other functionals, like statistical complexity, disequilibrium, etc.). An important issue is P itself is not a uniquely defined object and do exist several approaches to “associate” a given P with a given time series. Just to mention some extraction procedures frequently used in the literature: *a)* time series histogram [?], *b)* binary symbolic-dynamics [?], *c)* Fourier analysis [?], *d)* wavelet transform [?, ?], *e)* partition PDF [?], *f)* permutation PDF [?, ?], *g)* discrete PDF [?], etc. There is ample liberty to choose among them and the specific application must be analyzed to make a good choice.

The general procedure to assign P to a given time series consists in the following steps:

- (a) define an alphabet $\mathfrak{A} = \{s_j, j = 1, \dots, m\}$
- (b) convert the time series $X = \{x_i, i = 1, \dots\}$ into a *symbolic sequence* $A = \{a_i, a_i \in \mathfrak{A}\}$.
- (c) P is given by the relative frequencies of the symbols: $P = \{p_j, j = 1, \dots, m\}$ in the symbolic sequence A , where p_j is the relative frequency of symbol s_j .

P may be *non-causal* or *causal* [?] depending on step b. P is *non-causal* when one symbol $s_j \in \mathfrak{A}$ is assigned to each value $x_i \in X$. For example, the usual histogram technique used for time series of real numbers corresponds to this kind of assignment. Of course, in this method the temporal order of the time-series plays no role, and consequently the resulting P will not have any *causal information* and

the *symbolic sequence* may be simply regarded as a *coarse-grained* description of X [?]. It is also possible to group W consecutive values of the time series -a *trajectory* of length W - and assign one symbol to the group. Note that this procedure is equivalent to first assign a symbol to each value of the time series, then group W symbols into a *word* and finally construct a new alphabet consisting of words. If the original alphabet has m elements, there will be m^W possible words and one of this words will be assigned to the *trajectory* of W elements. P is given by the relative frequencies of all the possible words. Here P depends on the temporal order of X and consequently we call it a *causal* P . It is interesting to note that a *causal* P has information about statistics and also about temporal ordering of X . If a *non-causal* P is used instead, the analysis must be complemented with the evaluation of the Fourier transform, or the autocorrelation function of X , to recover the information about temporal ordering.

Let us stress even more the difference between a *non-causal* and a *causal* P by means of the following simple example. Let $X = \{x_i, i = 1, 2, \dots\}$ be a time series generated by *randn* (Matlab's[©] function); let $Y = \{y_i, i = 1, 2, \dots\}$ be the resulting series after a sorting process made by *sort* (Matlab's[©] function). Figs. 3.15.a and 3.15.b show the time series. One noncausal P is the normalized histogram, and $P(X)$ is identical to $P(Y)$ as Figures 3.15.c and 3.15.d reveal. One causal P may be obtained by the Bandt & Pompe procedure (for details about its determination see below) and Figs. 3.15.e and 3.15.f show that $P(X)$ and $P(Y)$ are completely different: $P(X)$ is almost uniform, reflecting X is randomly ordered, but $P(Y)$ has a delta-like shape, as far as Y is monotone increasing and only one ordering pattern is present.

Let us consider now the case of sampled digital signals like as sampled *RO*'s outputs are. Time series X is binary and has a natural alphabet with two symbols $\mathfrak{A} = \{0, 1\}$. The Shannon entropy of this alphabet is usually known as *Binary Entropy* S_2 . Suppose W consecutive bits of X are grouped into a *word*, that is the decimal number w_i between 0 and $2^W - 1$; consider these decimal numbers as the symbols of the new alphabet and let $Z = \{w_i, i = 1, 2, \dots\}$ be the new symbolic series. S_W is the entropy of $P_{hist}(Z)$ where subscript *hist* is for histogram; S_W is also known as *Block Entropy* of the binary time series X . Furthermore, if D consecutive decimal numbers w_i are grouped again and the $D!$ permutation patterns are considered as symbols of the new alphabet, we get a new $P_{BP}(Z)$, given by the relative frequencies of the permutation patterns. The entropy is $S_{BP}^{(D)}$, the *Bandt & Pompe entropy* [?] of the binary time series. All the above-mentioned entropies are given by the same Shannon famous formula:

$$S = - \sum_{j=1}^m p_j \log(p_j), \quad (3.8)$$

3.4. MEASURING THE JITTER OF RING OSCILLATORS BY MEANS OF INFORMATION TH

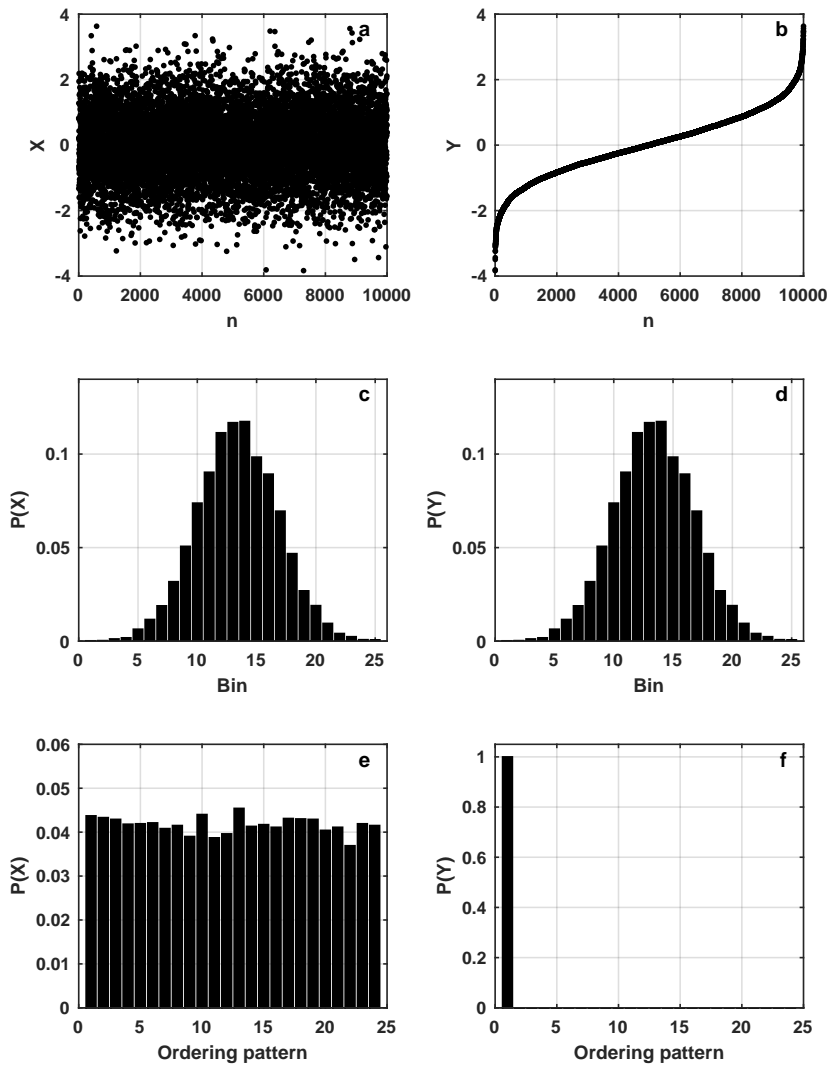


Figura 3.15: (see text) Time series X obtained by using function `randn` (a), its sorted version Y (b) and their causal (c, d) and non-causal histograms (e, f).

and the only difference between them is the P assigned to the time series. In this paper *log* means *base 2 logarithm*.

In this paper, we use a causal P determined with the Bandt & Pompe procedure. This procedure has been described in detail and successfully used in a number of papers concerning pseudo random number generation, system classifications, etc. [?, ?, ?, ?, ?, ?]. Let us summarize the basic procedure applied to our specific case:

- let $Z = \{w_i, i = 1, 2, \dots\}$ be a numerical time series (in our case W bits decimal numbers) series;
- choose an embedding dimension $D > 1$
- assign to each w_i a D -dimensional vector of previous $i, i-1, \dots, i-(D-1)$:

$$(s) \mapsto (w_{i-(D-1)}, w_{i-(D-2)}, \dots, w_{i-1}, w_i) \quad (3.9)$$

Clearly, the greater the D -value, the more information about “the past” is incorporated into these vectors.

- look for *ordinal patterns* of length D [?, ?, ?]. By “ordinal patternrelated to position i we mean the permutation $\pi = (r_0, r_1, \dots, r_{D-1})$ of $(0, 1, \dots, D-1)$ defined by

$$w_{i-r_{D-1}} \leq w_{i-r_{D-2}} \leq \dots \leq w_{i-r_1} \leq a_{i-r_0} \quad (3.10)$$

- In order to get a unique result consider that $r_j < r_{j-1}$ if $x_{i-r_j} = x_{i-r_{j-1}}$.
- Thus for all the $D!$ possible permutations π of order D is the probability distribution $P = \{p(\pi)\}$ defined by

$$p(\pi) = \frac{\#\{s | s \leq M - D + 1; i \text{ has type } \pi\}}{M - D + 1} \quad (3.11)$$

In the last expression, the symbol $\#$ stands for “number.” and corresponds to the number assigned to the permutation using the lexicographic order .

The main advantages of the Bandt & Pompe method are *a)* its simplicity, *b)* the extremely fast nature of the pertinent calculation-process, *c)* its robustness in the presence of observational and dynamical noise, and *d)* its invariance with respect to nonlinear monotonous transformations. The Bandt & Pompe methodology is not restricted to time series representative of low dimensional dynamical systems but can be applied to any type of time series (regular, chaotic, noisy, or reality

3.4. MEASURING THE JITTER OF RING OSCILLATORS BY MEANS OF INFORMATION TH

based), with a very weak stationary assumption (for $k = D$, the probability for $a_i < a_{i+k}$ should not depend on i [?]).

Let us stress some important issues involved in the calculations of the above-mentioned entropies:

1. The binary entropy S_2 is noncasual while both, the block entropy S_W and the Bandt & Pompe entropy $S_{BP}^{(D)}$, are causal.
2. The block entropy S_W takes into account correlations between W consecutive bits. Bandt & Pompe entropy $S_{BP}^{(D)}$ takes into account correlations between D consecutive W -length words. Both grouping procedures (decimal numbers of W bits and permutation patterns of D decimal numbers) may be done with or without superposition. The number of data required for good statistics is different depending the grouping procedures are made with superposition or not.
3. For S_W there is only one grouping process (W bits are grouped to obtain a decimal numbers time series Y). Let us define α as a statistical quality parameter, given by the quotient between the number of elements in the symbolic time series Y and the number of symbols in the alphabet. In this paper we will not accept $\alpha < 10$.

Obviously the quality factor α increases with the length of the time series:

- a) If the grouping of W bits is made with superposition, two consecutive W -length words share $W - 2$ bits. Consequently starting with a file with a length of N -bits we get $N - W + 1$ words. Furthermore, there are 2^W symbols in the alphabet and $\alpha = (N - W + 1)/(2^W)$.
- b) If S_W is evaluated without superposition the number of W -length words is $\text{floor}\{N/W\}$ and the quality parameter becomes $\alpha = \text{floor}\{N/W\}/(2^W)$. For $N \gg W$ the statistical quality factor is W times lower than the one with superposition.
4. In the case of $S_{BP}^{(D)}$, there are two grouping processes involved.
 - a) If both grouping processes are made with superposition we get $N - W - D + 2$ elements starting with a file N -bits length, and the quality factor is $\alpha = (N - W - D + 2)/D!$. In this case $S_{BP}^{(D)}$ takes into account the correlations between $W + D$ consecutive bits.
 - b) If the grouping process of W bits is made without superposition but the grouping of D decimal numbers is made with superposition we get $\text{floor}\{N/W\} - D + 1$ elements and the statistical quality parameter is

$\alpha = (\text{floor}\{N/W\} - D + 1)/D!$. In this case $S_{BP}^{(D)}$ will include correlations between WD consecutive bits.

- c) If the grouping process of W bits is made with superposition and the grouping of D decimal numbers is made without superposition we get $\text{floor}\{(N - W + 1)/D\}$ elements starting from a file with N bits. The statistical quality factor is $\alpha = \text{floor}\{(N - W + 1)/D\}/D!$ and $S_{BP}^{(D)}$ takes into account correlations between $W + D - 1$ bits.
- d) If both grouping processes are made without superposition we get $\text{floor}\{\text{floor}\{N/W\}/D\}$ elements starting from a N -bits length file. The statistical quality factor is $\alpha = \text{floor}\{\text{floor}\{N/W\}/D\}/D!$ and $S_{BP}^{(D)}$ takes into account correlations between WD consecutive bits.

Additional quantifiers

The Shannon Entropy $S(P)$ is the startpoint for other quantifiers:

1. Normalized entropy $H(P)$: it is the Shannon Entropy divided by its maximum value. For example, if we use S_2 (see above), the maximum entropy is obtained for equiprobability between two symbols. Its value is $S_{max} = -1/2\log(1/2) - 1/2\log(1/2) = \log(2) = 1$; then, the normalized entropy is $H_2 = S_2$. If we use S_W the equiprobability between the 2^W possible words (W -bits decimal numbers) produces $S_{max} = W$ and $H_W = S_W/W$. Finally for $S_{BP}^{(D)}$ the equiprobability between the $D!$ ordinal patterns produces $S_{max} = \log(D!)$ and $H_{BP}^{(D)} = S_{BP}^D/\log(D!)$.
2. Differential or conditional entropies h and h^* are:

$$h = S_{W+1} - S_W \quad (3.12)$$

$$h^* = S_{BP}^{(D+1)} - S_{BP}^{(D)} \quad (3.13)$$

In the above expressions $W = 1, 2, \dots$ and $D = 2, 3, \dots$, $S_0 = 0$ and $S_{BP}^{(1)} = 0$. These differential or conditional entropies give the average amount of information required to predict the $(W + 1)$ (or $(D + 1)$) symbol, given the preceding W (or D) symbols.

3. Finally the *rate entropies* h_0 and h_0^* are given by:

$$h_0 = \lim_{W \rightarrow \infty} h = \lim_{W \rightarrow \infty} S_W/W \quad (3.14)$$

$$h_0^* = \lim_{D \rightarrow \infty} h^* = \lim_{D \rightarrow \infty} S_{BP}^{(D)}/(D - 1) \quad (3.15)$$

3.4. MEASURING THE JITTER OF RING OSCILLATORS BY MEANS OF INFORMATION TH

Let us tell in advance that we shall show in section 3.4.4 that quantifiers S_W , $S_{BP}^{(D)}$, H_W and $H_{BP}^{(D)}$ are dependent on parameters W and D . This is a drawback if we want to use them as jitter measures. On the other hand, the estimators h and h^* of the *rate entropies* h_0 and h_0^* [?, ?] instead, are independent of W and D and we will show in Section 3.4.4 that in the case of sampled *RO*'s they also present a minimum for the correct sampling ratio making them good measure of the quality of both *RO*'s and *PRNG*'s derived from them.

3.4.4. Results

An evenly sampled output of a jitter-less *RO* was simulated with Matlab[©] and an output file with a length of $N_b = 7,000,000$ of bits was generated. A set of a hundred values of the sampling ratio $r = T_s/T \in [6,5,9,5]$, was explored (where T_s is the sampling period and T is the *RO* output period). Jitter with a normal distribution and a set with different values of variance σ_s (see below) were added to the original file. Our method emulates the real process of sampling the noisy output of a real *RO*; the detailed code is published in Mathworks[?].

For each value of σ_s , ten surrogates (each one with a different random initial condition) were generated and new files with N_b bits each were stored. It was assumed that jitter of individual samples is independent, normal distributed random variables, with zero mean value and variance $\sigma_i = \sigma_s$. Consequently, the variance of the accumulated jitter over one period T is given by $\sigma_T^2 = r\sigma_s^2$ [?]. The values considered are $\sigma_T = \{0, 0,001, 0,002, 0,003, 0,004, 0,005, 0,007, 0,01, 0,02, 0,02, 0,04, 0,05, 0,07, 0,1\}$.

For each file all the quantifiers defined in 3.4.3 were evaluated for $D \in [2, 10]$ and $W \in [1, 26]$. The details about evaluation, advantages and drawbacks of each quantifier are reported in section 3.4.3: they are S_W , $S_{BP}^{(D)}$, H_W , $H_{BP}^{(D)}$, h and h^* . Let us only show here the more relevant results to show the reason the last two quantifiers (h and h^*) are the best ones.

- In the case of normalized entropy H_W , it strongly depends on W . Furthermore the analysis of H_W as a function of r shows that it does not allow to determine an optimum value of the sampling ratio r (see Fig. 3.16). This is an important issue if the quantifiers are going to be used for experimental setups.
- In the case of the normalized Bandt & Pompe entropy $H_{BP}^{(D)}$, a strong dependence on the embedding dimension D is additionally present. Again it is not easy to determine the optimum value of r from the analysis of this parameter as a function of r (see Fig. 3.17).

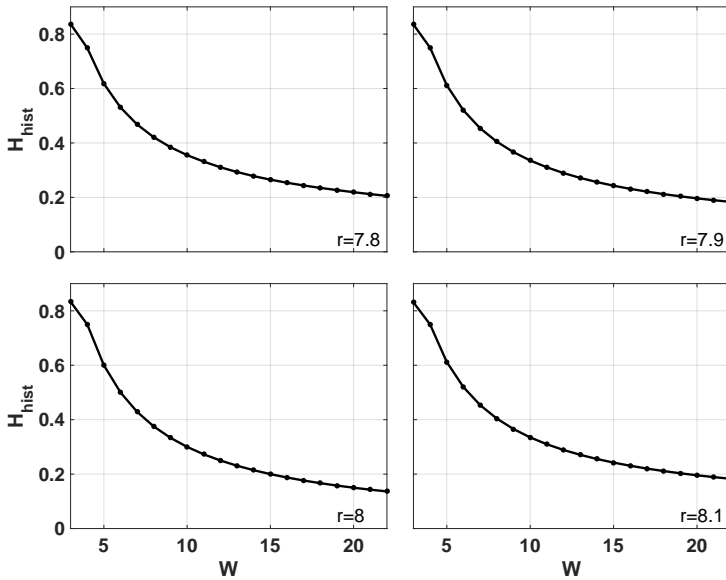


Figura 3.16: Normalized entropy H_W as a function of W for a jitter-less *RO* sampled with different values of r .

- A similar behavior appears in all the other functionals related with these two entropies. In summary, our results show that both h y h^* are independent of any arbitrary parameter used in their statistical determination. These two quantifiers have also been considered in two excellent articles [?, ?].

Our results show that two quantifiers, h and h^* , are appropriate to be used as jitter measures because:

- (a) for $\sigma_T = 0$ (jitter-less output) they rapidly approach to a constant limiting value as both D and W increase toward ∞ and this limiting value is independent of both D and W ;
- (b) they are increasing monotone (and almost proportional) functions of σ_T .
- (c) From their analysis, it is possible to detect the optimum value of the sampling ratio r . Let us show these claims in the following figures that are representative of all our results.

Figure 3.18 shows the Bandt & Pompe differential entropy h^* , as a function of D , with W as a parameter, for a ring without jitter. It can be seen that there is a

3.4. MEASURING THE JITTER OF RING OSCILLATORS BY MEANS OF INFORMATION TH

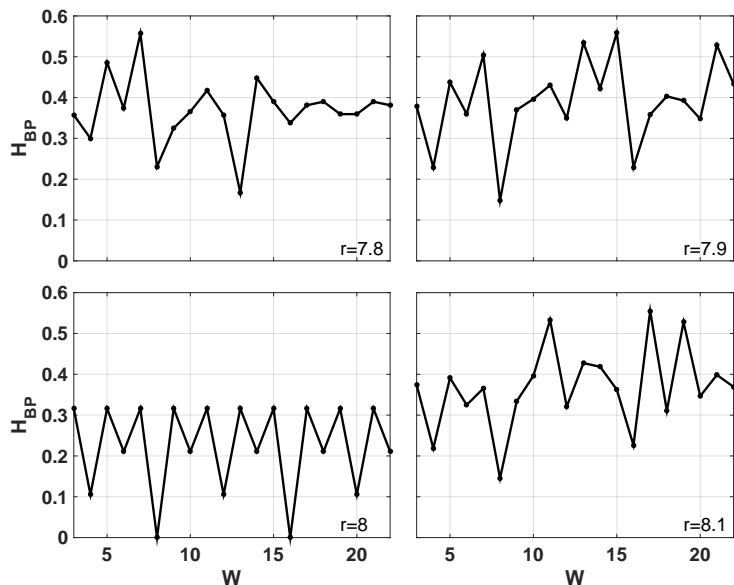


Figura 3.17: $H_{BP}^{(D)}$ as a function of W for a jitter-less RO sampled with different values of r . Calculations are made without superposition of words

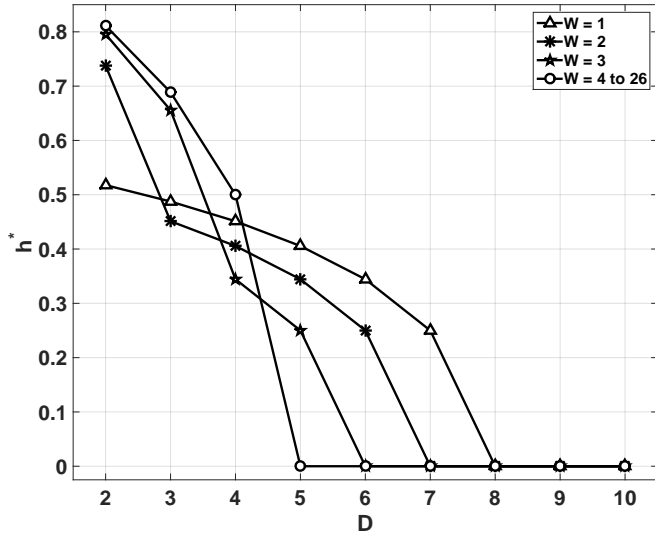


Figura 3.18: h^* as a function of D for a jitter-less RO sampled with $r = 8$.

threshold value $W = 4$ over which all the curves collapse into one for every value of D . Furthermore, Fig. 3.18 also shows that for $D \geq 8$ all the curves collapse into one, regardless the value of W . In conclusion, if $D \geq 8$ and $W \geq 4$ one obtains a quantifier independent of both D and W . The influence of jitter on this quantifier is shown in Figure 3.19, where h^* is plotted as a function of D with σ_T as a parameter. The values considered are $\sigma_T = \{0(\text{no jitter}), 0,001, 0,002, 0,003, 0,004, 0,005, 0,007, 0,01, 0,02, 0,02, 0,04, 0,05, 0,07, 0,1\}$. The inset of Fig. 3.19 shows h^* as a function of σ_T for $D = 8$. This inset shows that this quantifier is an increasing monotone function of σ_T . Finally Fig. 3.20 shows h^* as a function of the sampling ratio r . In this figure, it is shown that there is a minimum for the right r (in this case $r = 8$). Furthermore sensitivity of h^* as a function of jitter is maximum for this same ideal value of r .

Let us now analyze the second quantifier, h . This quantifier only depends on W because D is not used to define the PDF assigned to the data series. Fig. 3.21 shows jitter-less case, h is almost independent of W for $W \geq 4$. In this paper, we adopted $W = 6$. Figure 3.22 shows the influence of jitter over this quantifier. It is clear from the inset in this figure that, for the selected value $W = 6$, h is an increasing monotone function of jitter variance σ_T .

Fig. 3.23 shows that h has a minimum when the value of r takes its optimum

3.4. MEASURING THE JITTER OF RING OSCILLATORS BY MEANS OF INFORMATION TH

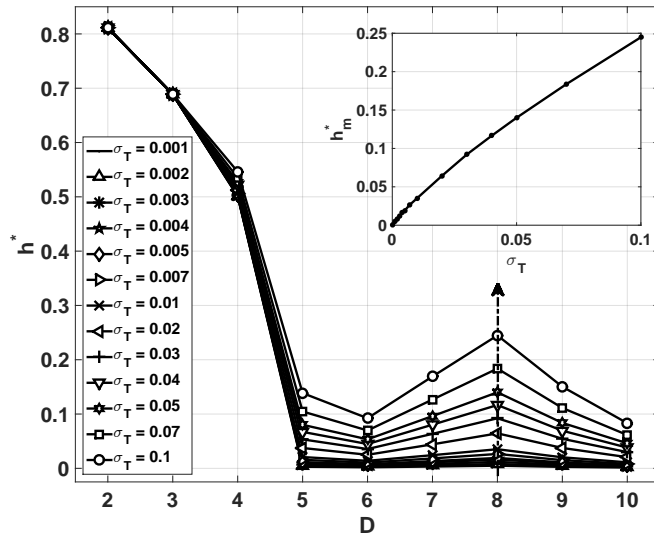


Figura 3.19: h^* as a function of D for a *RO* sampled with $r = 8$ for a world length $W = 6$ for jitter with several variances. The inset shows h^* as a function of σ_T for $r = 8$, $W = 6$ and $D = 8$.

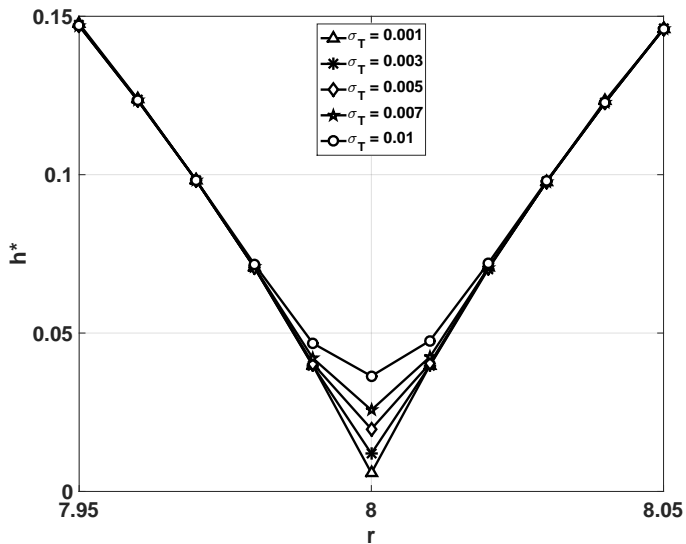


Figura 3.20: h^* as a function of r for $r \in [7.95, 8.05]$, with several σ_T , $W = 6$ and $D = 8$. The curve has a minimum at the correct value $r = 8$.

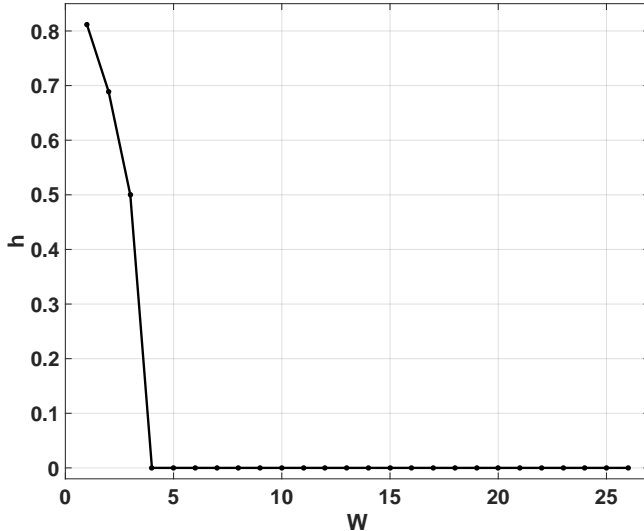


Figura 3.21: h as a function of W for a jitter-less RO sampled with $r = 8$.

value ($r = 8$). Note that this minimum is robust also in the presence of jitter.

Further analysis must be done to assure that the selected values $W = 6$ and $D = 8$ produce symbolic files with a good statistics. For a given alphabet \mathcal{A} with m elements, and a given symbolic file of length n , the quality parameter $\alpha = n/m$, see 3.4.3. Quality is better as α increases and a minimum value $\alpha = 10$ was accepted. According to section 3.4.3 the selected values $W = 6$ and $D = 8$ provide $\alpha_h \simeq 10^5$, $\alpha_{h^*} \simeq 175$ with superposition and 29 without superposition. All cases give $\alpha > 10$ as required.

A comparison between both quantifiers is shown in Figure 3.24. Markers correspond to variances $\sigma_T = \{0, 0,001, 0,002, 0,003, 0,004, 0,005, 0,007, 0,01, 0,02, 0,03, 0,04, 0,05, 0,07, 0,1\}$. Note that the slope of any of these curves is dh^*/dh and it is equal to the quotient between slopes of curves in the insets of Figs. 3.19, and 3.22. If $dh^*/dh > 1$, h^* is more sensitive than h to measure jitter. The slope slightly increases from $\sim 2,47$ for $W = 5$ to $\sim 5,54$ for $W = 19$ showing that h^* becomes more sensitive as W increases.

We also evaluated h^* without the superposition of bits between consecutive natural numbers but keeping the superposition of $D - 1$ natural numbers between ordering patterns (In all cases h was evaluated with superposition of $W - 1$ consecutive bits). Results are depicted in Fig. 3.25 where it is shown that removing

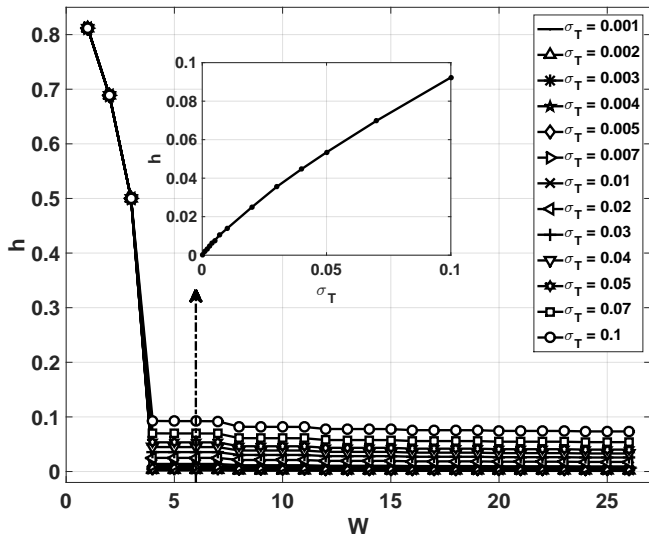


Figura 3.22: h as a function of W for a RO sampled with $r = 8$, for jitter with several variances. The inset shows h as a function of σ_T for $r = 8$ and $W = 6$.

3.4. MEASURING THE JITTER OF RING OSCILLATORS BY MEANS OF INFORMATION TH

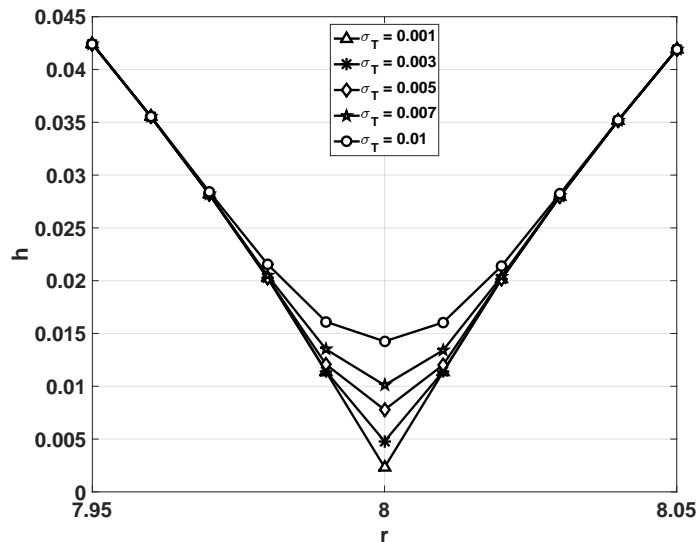


Figura 3.23: h as a function of r for $r \in [7.95, 8.05]$, with several σ_T and $W = 6$. The curve has a minimum at the optimum value $r = 8$.

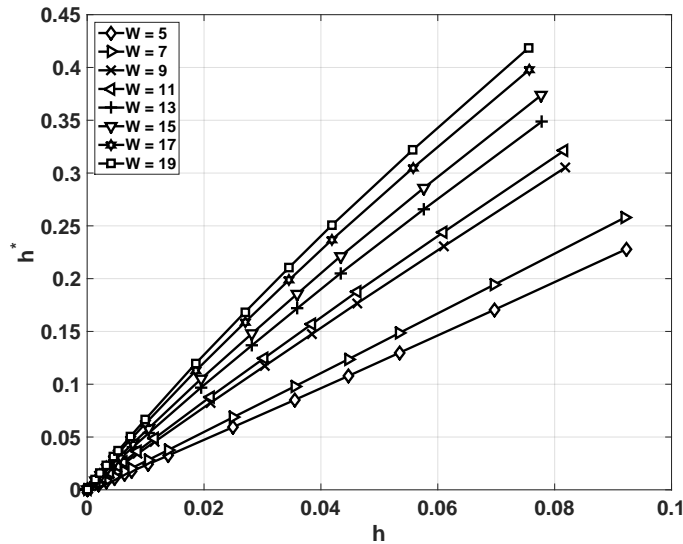


Figura 3.24: h^* as a function of h for $r = 8$, $D = 8$ and different values of W .

the superposition the sensitivity of this quantifier increases. Of course, we get a smaller amount of W bits natural numbers form the original seven million binary file, and consequently, the statistical quality is lower than that of the original calculation with superposition. To increase α up to its previous value, longer binary files are required.

3.4.5. Conclusions

Given their usefulness as *PRNG* and clock generators, *ROs* are becoming one of the main building blocks of digital circuits. Jitter is unavoidable in *ROs*, and consequently, it needs to be characterized. Mixing and distribution of values are the main properties to consider. Several *ITQ* quantifiers were evaluated here. S_W , $S_{BP}^{(D)}$, H_W and $H_{BP}^{(D)}$ turn out to be dependent on parameters W and D . This is a drawback if we use them as jitter measures. On the other hand, it is no possible to calculate *rate entropies*, h_0^* and h_0 , since an infinite number of data is necessary for their calculation. The two *differential entropies*, h^* and h , instead, are independent of the parameters used for their determination and are estimators of the *rate entropies*. We have shown in Section 3.4.4 that in the case of sampled *ROs* they also present a minimum for the correct sampling ratio making them a

3.4. MEASURING THE JITTER OF RING OSCILLATORS BY MEANS OF INFORMATION TH

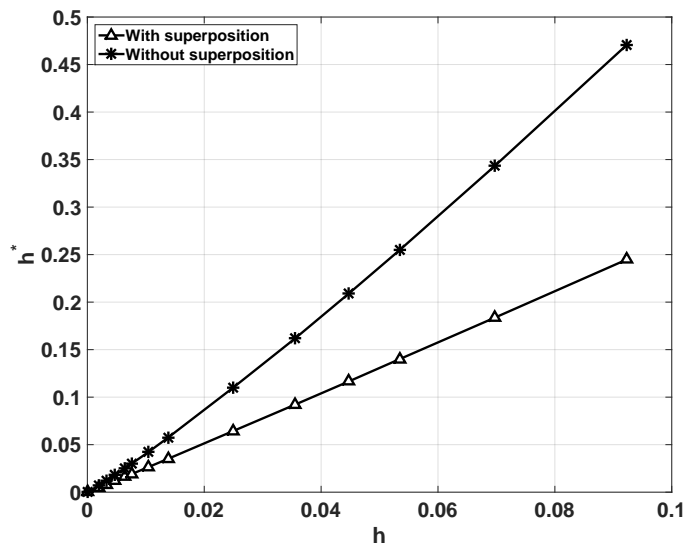


Figura 3.25: h^* as a function of h for $r = 8$, $W = 6$ and $D = 8$. Two procedures to obtain W -bits natural numbers are considered: with and without superposition (see text).

good measure of the quality of both *RO*'s and *PRNG*'s derived from them.

The dual entropy plane determined by these quantifiers has demonstrated to satisfactorily discern between the *PRNG*'s two main desired properties, the equi-probability among all possible values and the statistical independence between consecutive values. Thus, it allows clearly seeing what needs to be improved in a given sequence. The examples presented here have demonstrated the need to use both histograms for characterizing sequences.

Capítulo 4

El problema de la Aritmética Discreta

4.1. Analysis of the digital implementation of a chaotic deterministic-stochastic attractor (EAM- TA 2012)

Otro que no tengo el latex, se lo tengo que pedir a Luciana

In this work the implementation, of chaos-based pseudo random number generators (PRNG), onto a Field Programmable Gate Array (FPGA), is analyzed. Any digital implementation requires the choice of an algorithm to discretize time and a representation standard to represent real numbers. Each choice modifies the stochasticity degree of the system and also defines a different amount of resources on the FPGA. The main contribution of this paper is to propose an optimum design methodology for applications in which the chaotic system is going to replace a stochastic system. This is the case with PRNG. In stochastic systems the randomness degree must be measured. In this paper we use the global indicator proposed by Marsaglia in his widely used DIEHARD tests-suite. Results are exemplified for the Lorenz chaotic oscillator but the same methodology may be used with other low dimensional chaotic systems.

4.2. Complexity of switching chaotic maps

4.2.1. Introduction

In the last years digital measuring systems become the standard in all experimental sciences. By using *virtual instruments* and new programmable electronic devices, such as Digital Signal Processors (*DSP*) and Field Programmable Gate Arrays (*FPGA*) experimenters may design and modify their own measuring systems.

The effect of finite precision in these new devices needs to be investigated. This issue is critical if chaotic systems must be implemented, because due to roundoff errors digital implementations will always become periodic with a period T and unstable orbits with a low period may become stable destroying completely the chaotic behavior. Grebogi and coworkers [?] studied this subject and they shaw that the period T scales with roundoff ϵ as $T \sim \epsilon^{-d/2}$ where d is the correlation dimension of the chaotic attractor.

To have a large period T is one an important property of a chaotic map. Stochasticity and mixing are also relevant. Furthermore to characterize these properties several quantifiers were studied [?]. Among them the use of an entropy-complexity representation ($H - C$ plane) deserves special consideration[?, ?, ?, ?, ?]. A fundamental issue is the criterium to select the distribution function (*PDF*) assigned to the time series. Causal and non causal options are possible. Here we consider the non-causal traditional *PDF* obtained by normalization of the histogram of the time series. Its statistical quantifier is the normalized entropy H_{hist} that is a measure of equiprobability among all allowed values. We also consider a causal *PDF* that is obtained by assigning ordering patterns to segments of trajectory of length D . This PDF were first proposed by Bandt & Pompe in a seminal paper [?]. The corresponding entropy H_{BP} was also proposed as a quantifier by Bandt & Pompe. Amigó and coworkers proposed the number of forbidden patterns as a quantifier of chaos [?]. Essentialy they reported the presence of forbidden patterns as an indicator of chaos. Recently it was shown that the name forbidden patterns is not convenient and it was replaced by *missing patterns*(MP) [?].

Switching systems naturally arise in power electronics and many other areas in digital electronics. They have also interest in transport problems in deterministic ratchets [?] and it is known that synchronization of the switching procedure affects the output of the controlled system. Nagaraj et al [?] studied the case of switching between two maps. They shaw that the period T of the compound map obtained by switching between two chaotic maps is higher than the period of each map. Liu et al [?] studied different switching rules applied to linear systems to generate chaos. Switching chaos was also addressed in [?]. Skipping values of the time series

is another simple technique used to increase mixing in chaotic maps [?].

In this paper we study the statistical characteristic of two well known maps: the tent map (TENT) and logistic map (LOG). Three additional maps are generated: 1) SWITCH, generated by switching between TENT and LOG; 2) EVEN, generated by skipping all the elements in odd position in SWITCH time series and 3) ODD, generated by discarding all the elements in an even position in SWITCH time series. Floating point, decimal numbers and binary numbers are used. All these specific numerical systems may be implemented in modern programmable logic boards.

The main contributions of this paper are:

1. the definition of different statistical quantifiers and their relationship with the properties of the time series generated by the map.
2. the study of how these quantifiers are modified by the numerical representation using floating point, decimal and binary numbers. It is specially interesting to note that some systems (TENT) with very nice statistical properties in the world of the real numbers, become “pathological” when numerical representations are used.
3. the effect of switching between two different maps, on the period and the statistical properties of the time series. Floating point, decimal and binary numerical representations are considered.
4. the effect of skipping values in any of these maps

Organization of the paper is as follows: section 3.4.3 describes the statistical quantifiers used in the paper and the relationship between their value and characteristics of the causal and non causal PDF considered; section 4.2.3 shows and discuss the results obtained for all the numerical representations. Finally section 4.2.5 deals with final remarks and future work.

4.2.2. Information theory quantifiers

The first step to quantify the statistical properties of the values (amplitude statistics) of a time series $\{x_i, (i = 1, \dots, N)\}$, using information theory is to determine the concomitant PDF because all the quantifiers are functionals of the PDF associated to the time series. This is an issue studied in detail in previous papers [?]. Let us summarize the procedure:

1. a finite alphabet with M symbols $\mathbf{A} = \{a_1, \dots, a_M\}$ is chosen.
2. one of these symbols is assigned: (a) to each value of the time series or (b) to each portion of length D of the trajectory.

3. the normalized histogram of the symbols is the desired *PDF*.

Note that if option (a) is chosen in step 2 then the PDF is *non causal*, because all the information about the time evolution of the system generating $\{x_i\}$ is completely lost. On the contrary if option (b) is chosen in step 2 then the PDF is *causal*, in the sense it has some information about the temporal evolution.

Of course there are infinite possibilities to choose the alphabet \mathbf{A} as well as the length D . Bandt & Pompe made a proposal for a causal PDF that has been shown to be easy to implement and useful in a great variety of applications. The procedure is the following [?, ?, ?]:

- Given a series $\{x_t : t = 0, \Delta t, \dots, M\Delta t\}$, a sequence of vectors of length d is generated.

$$(s) \mapsto (x_{t-(d-1)\Delta t}, x_{t-(d-2)\Delta t}, \dots, x_{t-\Delta t}, x_t) , \quad (4.1)$$

Each vector turns out to be the “history” of the value x_t . Clearly, the longer the length of the vectors D , the more information about the history would the vectors have but a higher value of N is required to have an adequate statistics.

- The permutations $\pi = (r_0, r_1, \dots, r_{D-1})$ of $(0, 1, \dots, D-1)$ are called “order of patterns” of time t , defined by:

$$x_{t-r_{D-1}\Delta t} \leq x_{t-r_{D-2}\Delta t} \leq \dots \leq x_{t-r_1\Delta t} \leq x_{t-r_0\Delta t}. \quad (4.2)$$

In order to obtain an unique result it is considered $r_i < r_{i-1}$ if $x_{t-r_i\Delta t} = x_{t-r_{i-1}\Delta t}$.

In this way, all the $D!$ possible permutations π of order D , and the PDF $P = \{p(\pi)\}$ is defined as:

$$p(\pi) = \frac{\#\{s | s \leq M - D + 1; (s) \text{ has type } \pi\}}{M - D + 1}. \quad (4.3)$$

In the last expression the $\#$ symbol means “number”.

This procedure has the advantages of being *i*) simple, *ii*) fast to calculate, *iii*) robust in presence of noise, and *iv*) invariant to lineal monotonous transformations.

It is applicable to weak stationarity processes (for $k = D$, the probability that $x_t < x_{t+k}$ doesn't depend on the particularity t [?]). The causality property of the PDF allows the quantifiers (based on this PDFs) to discriminate between deterministic and stochastic systems [?].

According to this point Bandt and Pompe suggested $3 \leq D \leq 7$. $D = 6$ has been adopted in this work.

Based on our previous research [?, ?] we have employed two *PDF*'s: (a) the normalized histogram of the time series amplitudes $\{x_i\}$ (that is a non-causal *PDF*), and (b) the Bandt & Pompe *PDF* (that is a causal *PDF*). The entropies H_{hist} and H_{BP} , the statistical complexity C_{BP} are used as quantifiers.

We also used the number of missing patterns MP as a quantifier[?]. As shown recently by Amigó *et al.* [?, ?, ?, ?], in the case of deterministic one-dimensional maps, not all the possible ordinal patterns can be effectively materialized into orbits, which in a sense makes these patterns “forbidden”. Indeed, the existence of these *forbidden ordinal patterns* becomes a persistent fact that can be regarded as a “new” dynamical property. Thus, for a fixed pattern-length (embedding dimension D) the number of forbidden patterns of a time series (unobserved patterns) is independent of the series length N . Remark that this independence does not characterize other properties of the series such as proximity and correlation, which die out with time [?, ?].

A full discussion about the convenience of using these quantifiers is out of the scope of this work. Nevertheless reliable bibliographic sources do exist [?, ?, ?, ?, ?, ?, ?].

The entropies H_{hist} and H_{BP} are the normalized version of the Of course there are infinite possibilities to choose the alphabet as well as the length d . Bandt & Pompe made a proposal for a causal PDF that has been shown to be easy to implement and useful in a great variety of applications. The procedure is the following [?, ?, ?]: a) Given a series $\{x_t : t = 0, \Delta t, \dots, M\Delta t\}$, a sequence of vectors of length d is generated.

$$(s) \mapsto (x_{t-(d-1)\Delta t}, x_{t-(d-2)\Delta t}, \dots, x_{t-\Delta t}, x_t) , \quad (4.4)$$

Each vector turns out to be the “history” of the value x_t . Clearly, the longer the length of the vectors d , the more information about the history would the vectors have. b) The permutations $\pi = (r_0, r_1, \dots, r_{d-1})$ of $(0, 1, \dots, d-1)$ are called “order of patterns” of time t , defined by:

$$x_{t-r_{d-1}\Delta t} \leq x_{t-r_{d-2}\Delta t} \leq \dots \leq x_{t-r_1\Delta t} \leq x_{t-r_0\Delta t}. \quad (4.5)$$

In order to obtain an unique result it is considered $r_i < r_{i-1}$ if $x_{t-r_i\Delta t} = x_{t-r_{i-1}\Delta t}$.

In this way, all the $d!$ possible permutations π of order d , and the PDF $P = \{p(\pi)\}$ is defined as:

$$p(\pi) = \frac{\#\{s | s \leq M - Dd + 1; (s) \text{ has type } \pi\}}{M - d + 1}. \quad (4.6)$$

In the last expression the $\#$ symbol means “number”.

This procedure has the advantages of being *i*) simple, *ii*) fast to calculate, *iii*) robust in presence of noise, and *iv*) invariant to lineal monotonous transformations.

It is applicable to weak stationarity processes (for $k = d$, the probability that $x_t < x_{t+k}$ doesn't depend on the particulary t [?]). The causality property of the PDF allows the quantifiers (based on this PDFs) to discriminate between deterministic and stochastic systems [?].

The choice of the embedding dimension d is crucial because it determines the minimal length acceptable of the original temporal series ($M \gg d!$) needed to obtain an adequate statistics. According to this point Bandt and Pompe suggested $3 \leq d \leq 7$. $d = 6$ has been adopted in this work.

Based on our previous research [?] we have employed the statistical complexity C and the entropy H to define a plane where the stochasticiy of the chaotic system may be represented. A full discussion about the convenience of using these quantifiers is out of the scope of this work. Nevertheless reliable bibliographic sources do exist [?, ?, ?, ?, ?, ?, ?].

The entropy $H[P]$ is the normalized version of the Entropy proposed by Shannon [?]:

$$H[P] = S[P]/S_{max}, \quad (4.7)$$

where $S[P] = -\sum_{j=1}^M p_j \ln(p_j)$

and S_{max} is the normalizing constant:

$$S_{max} = S[P_e] = \ln M, \quad (4.8)$$

and $P_e = \{1/M, \dots, 1/M\}$ is the uniform distribution. The number of symbols M is equal to N for H_{hist} and it is equal to $D!$ for H_{BP} .

The statistical complexity $C[P]$ is given by:

$$C[P] = Q_J[P, P_e] \cdot H[P], \quad (4.9)$$

, and Q_J is named “disequilibrium” and it is the distance between P and P_e in the probability space. The metric used in this paper is based on the Jensen-Shannon divergence [?]:

$$Q_J[P, P_e] = Q_0 \cdot \left\{ S\left[\frac{P + P_e}{2}\right] - S[P]/2 - S[P_e]/2 \right\}. \quad (4.10)$$

The normalization constant Q_0 is:

$$Q_0 = -2 \left\{ \left(\frac{N+1}{N} \right) \ln(N+1) - 2 \ln(2N) + \ln N \right\}^{-1}. \quad (4.11)$$

From the statistical point of view the disequilibrium Q_J is an intensive magnitude, and it is 0 if and only if $P = P_e$. It has been proved that the $C[P]$ quantifies

the presence of nonlinear correlations typical of chaotic systems [?, ?]. The complexity $C[P]$ is independent from the entropy $H[P]$, as far as different P 's share the same entropy $H[P]$ but they have different complexity $C[P]$.

Two representation planes are considered: H_{BP} vs H_{hist} [?] and H_{BP} vs C_{BP} [?]. In the first plane a higher value in any of the entropies, H_{BP} and H_{hist} , implies an increase in the uniformity of the involved *PDF*. The point $(1, 1)$ represents the ideal case with uniform histogram and uniform distribution of ordering patterns. In the second plane not the entire region $0 < H_{BP} < 1, 0 < C_{BP} < 1$ is achievable. In fact for any *PDF* the pairs (H, C) of possible values fall between two extreme curves in the plane H - C [?]. Fig. ?? shows two regions labeled as *deterministic* and *stochastic*. In fact transition from one region to the other are smooth and the division is a bit arbitrary. A more detailed discussion can be seen in [?]. Ideal random systems having uniform Bandt & Pompe *PDF*, are represented by the point $(1, 0)$ [?] and a delta-like *PDF* corresponds with the point $(0, 0)$.

4.2.3. Results

Five pseudo chaotic maps were studied. For each one a floating point representation, a decimal numbers representation with $1 \leq P \leq 27$ and a binary numbers representation with $1 \leq B \leq 27$ are considered. For each representation 1000 time series were generated using randomly chosen initial conditions within the interval $[0, 1]$. The studied maps are tent (TENT), logistic (LOG) a sequential switching between TENT and LOG (SWITCH). Furthermore a skipping randomization procedure is applied to SWITCH [?], discarding the values in the odd positions (EVEN) or the values in the even positions (ODD) respectively. Let us detail our results for each of these maps.

4.2.4. Simple maps.

Here we report our results for both maps:

1. Tent map (TENT)

$$x_{n+1} = \begin{cases} 2x_n & \text{if } 0 \leq x_n \leq 1/2 \\ 2(1-x_n) & \text{if } 1/2 < x_n \leq 1 \end{cases}, \quad (4.12)$$

with $x_n \in \mathcal{R}$. The Tent map has been extensively studied in the literature because theoretically it has nice statistical properties that can be analytically obtained. For example it is easy to proof that it has a uniform histogram and consequently an ideal $H_{hist} = 1$. The Perron-Frobenius operator and its corresponding eigenvalues and eigenfunctions may be also be analytically obtained for this map [?].

When this map is implemented in a computer using any numerical representation system (even floating point!) truncation errors rapidly increases and makes the unstable fixed point in $x^* = 0$ becomes stable producing a short transitory followed by an infinite number of 0's [?, ?]. Some authors [?] have proposed to add a random perturbation to avoid this drawback of the Tent map. But this procedure introduces statistical properties of the random perturbation that are mixed with those of the Tent map itself.

Here we study the Tent map “as it is” without any artifact to evaluate its real instead of theoretical statistical properties. Note that to effectively work in a given representation it is necessary to change the expression of the map in order to make all the operations in the chosen representation numbers. For example, in the case of TENT the expression in decimal numbers is:

$$x_{n+1} = \begin{cases} 2x_n & \text{if } 0 \leq x_n \leq 1/2 \\ \epsilon \times \text{floor}\left\{\frac{2 - 2x_n}{\epsilon}\right\} & \text{if } 1/2 < x_n \leq 1 \end{cases}, \quad (4.13)$$

with $\epsilon = 10^{-P}$ for decimal numbers and $\epsilon = 2^{-B}$ for binary numbers. In Eq. 4.13 x_n is either a decimal number with P digits or a binary number with B bits.

Figs. 4.3 (a) to (e) show the different quantifiers for floating point and decimal numerical representation. In each figure from (a) to (c) a dashed line shows the value for the floating point representation. In figures (d) and (e) the star corresponds to the floating point case. In decimal representations the value of H_{hist} remains almost constant for $11 \leq P \leq 16$ (see Fig. 4.3 (a)). Its value is $\langle H_{hist} \rangle = 0,8740$ with a variance $\sigma_{H_{hist}} = 2,5 \times 10^{-6}$. For lower or higher values pf P entropy decreases. This effect is due precisely to the stabilization of the fixed point at $x = 0$. For ordering patterns entropy H_{BP} an almost constant value is obtained for $8 \leq P \leq 15$. The value is $H_{BP} \simeq 0,6287$ with variance $\sigma_{H_{BP}} = 4,8 \times 10^{-6}$ (see Fig. 4.3 (b)). This rather small maximum value may be understood by seeing Fig. 4.3 (c), where the number of MP. is minimal for P within the same range but it is still large: 645 patterns are missing and only 75 ordering patterns are present in the time series. Then, even with a uniform distribution between these 75 patterns, entropy can not be higher than $\ln(75)/\ln(720) \simeq 0,65$. A more complete perspective of the statistical properties is obtained in Fig. 4.3 (d) showing the representative point in the H_{hist}, H_{BP} plane for different precisions. Note that the best choice for maximum stochasticity is obtained for $11 \leq P \leq 15$, with maximum attainable values for both entropies. Increasing the number of decimal figures makes Tent map worst in the sense the system approaches the state for the floating point representation (the star at $(0,0)$). Statistical complexity C_{BP} is also maximal for $8 \leq P \leq 15$. Fig.

4.3 (e) shows the representation on the H_{BP}, C_{BP} plane. In this plane it is also clear that the more stochastic option corresponds with $11 \leq P \leq 15$ but even in the optimum case the representative point is located in a position very similar to other chaotic maps, very far from the ideal point for stochastic systems in this plane that is $(1, 0)$ [?]. Binary numerical representation of the Tent map remains very near to the floating point values for $1 \leq B \leq 27$ (see Fig. 4.3 (f)). The conclusion is it is convenient to use a decimal numbers representation with $P = 11$ to get the optimum time series for the Tent map. A higher number of decimal figures does not improve the statistical properties of the time series. Furthermore binary and floating point representations are not allowed.

2. Logistic map (LOG) Logistic map is representative of the very large family of quadratic maps.

$$x_{n+1} = 4 x_n (1 - x_n), \quad (4.14)$$

with $x_n \in \mathcal{R}$. Figs. 4.4 (a) to (f) show the statistical properties of LOG map in floating point and decimal numbers representation. This map does not show the anomalies pointed above for the tent map. For $P \geq 10$ the values of H_{hist} , H_{BP} and C_{BP} remains almost identical to the values for the floating point representation. Their values are: $\langle H_{hist} \rangle = 0,8621$ with variance $\sigma_{H_{hist}} = 0,062 \times 10^{-6}$; $\langle H_{BP} \rangle = 0,6292$ with variance $\sigma_{H_{BP}} = 0,060 \times 10^{-6}$; $\langle C_{BP} \rangle = 0,4842$ with variance $\sigma_{C_{BP}} = 0,0195 \times 10^{-6}$. Missing patterns stabilize in 645 for $P \geq 8$ making H_{BP} to rise to its floating point value $\langle H_{BP} \rangle = 0,629$ with variance $\sigma_{H_{BP}} = 0,060 \times 10^{-8}$. Note again that the stable value of mission patters missing patterns 645 makes the optimum $H_{BP} \leq \ln(75)/\ln(720) \simeq 0,65$. Then $P = 10$ is the most convenient choice because an increase in the number of decimal figures does not improve the statistical properties. Figs. ?? show the corresponding figures for binary representations. The histogram entropy H_{hist} does not reach its floating point value within the maximum number of bits used. In the case of missing patterns the stable number 645 is obtained with $B \geq 25$. It means that using $B = 25$ one obtains a time series with good statistical properties regarding the missing patterns, but distribution among the allowed binary values is not as uniform as can be obtained with a higher value of B .

In summary, a comparison between LOG and TENT maps shows that, in the case of decimal representation, the best choice for TENT ($P = 11$) produces a higher value for H_{hist} than the best choice for LOG ($P = 10$). Ordering patterns and the statistical properties related to them, are almost identical for the optimum choices in both maps. In the case of binary numbers only LOG can be used because TENT is highly anomalous.

Sequential switching

1. Sequential switching between Tent and Logistic maps (SWITCH) SWITCH may be expressed as a composition between $M_1 \circ M_2$ given by the following recurrence:

$$\begin{cases} x_{n+2} = 4 x_{n+1} (1 - n + 1) \\ x_{n+1} = \begin{cases} 2 x_n & \text{if } 0 \leq x_n \leq 1/2 \\ 2 (1 - x_n) & \text{if } 1/2 < x_n \leq 1 \end{cases} \end{cases}$$

with $x_n \in \mathcal{R}$. Results with sequential switching are shown in Figs. 4.6 (a) to (f) for decimal numbers. The floating point entropy value is $H_{hist} = 0,8658$, a value very similar to the one obtained for the TENT map and higher to that obtained for LOG. For decimal numbers this value is reached for $12 \leq P \leq 27$. It means it is enough to use 12 decimal figures to get the same distribution of values in the time series. Regarding ordering patterns the number of MP decreases to 586, a value lower than the one obtained for any of two simple maps TENT and LOG. It means the entropy H_{BP} may increase up to $\ln(134)/\ln(720) \simeq 0,74$ With decimal numbers the entropy H_{BP} stabilizes at $P = 9$ with $\langle H_{BP} \rangle \simeq 0,657$ and variance $\sigma_{H_{BP}} \simeq 0,13 \times 10^{-7}$. Note that the entropies H_{hist} and H_{BP} are not monotonously increasing with P . Considering all the quantifiers $P = 12$ is the minimum number of decimal figures and statistical characteristics of this combined map are better than those for each individual map. Results with sequential switching in binary numbers are shown in Figs. 4.7. Results for a number of bits $B \simeq 27$ are equivalent to those obtained for $P \simeq 9$ for decimal numbers. It means both representation are valid and equivalent in the sense they will require similar hardware resources.

2. Skipping is a usual randomizing technique that increases the mixing quality of a single map and correspondingly increases the value of H_{BP} and decreases C_{BP} of the time series. Skipping does not change the values of H_{hist} and C_{hist} evaluated using the non causal PDF (normalized histogram)[?]. In the case under consideration we study Even and Odd skipping of the sequential switching of Tent and Logistic maps.
 - a) Even skipping of the sequential switching of Tent and Logistic maps (EVEN).
If $\{x_n, (n = 1, \dots, \infty)\}$ is the time series generated by 1 discard all the values in odd positions and retain the values in even positions.
 - b) Odd skipping of the sequential switching of Tent and Logistic maps.
If $\{x_n, (n = 1, \dots, \infty)\}$ is the time series generated by 1 discard all the values in even positions and retain all the values in odd positions.

The reason for studying even and odd skipping cases is the sequential switching map M_{switch} is the composition of two different maps. Even skipping may be expressed as $M_{TENT} \circ M_{LOG}$ while odd skipping may be expressed as $M_{LOG} \circ M_{TENT}$.

This is very interesting to note that a great improvement is obtained using any of the skipping strategies but EVEN is slightly better than ODD.

MP are reduced to $MP \simeq 163$ for EVEN and $MP \simeq 164$ for ODD, increasing the maximum allowed Bandt & Pompe entropy that reaches the mean value $\langle H_{BP} \rangle \simeq 0,905$ with variance $\sigma_{H_{BP}} \simeq 0,107 \times 10^{-6}$ for EVEN, and $\langle H_{BP} \rangle \simeq 0,854$ with variance $\sigma_{H_{BP}} \simeq 0,285 \times 10^{-6}$ for a decimal representation with $9 \leq P \leq 27$. The complexity is reduced to $\langle C_{BP} \rangle \simeq 0,224$ with $\sigma_{C_{BP}} \simeq 0,166 \times 10^{-6}$ for EVEN and $\langle C_{BP} \rangle \simeq 0,282$ with $\sigma_{C_{BP}} \simeq 0,281 \times 10^{-6}$ for ODD.

Quantifiers related to the normalized histogram slightly degrades with the skipping procedure. For example H_{hist} reduces from 0,866 without skipping to 0,813 for any EVEN or ODD.

Results in binary numbers are similar to those obtained for the equivalent number of figures in decimal numbers. For example the minimum in MP is reached for $B = 27$, and this number of bits is almost equivalent to $P = 9$.

In Figs. 4.8 and Figs. 4.9 are shown the results for EVEN. We do not give the Figs. for ODD because they are very similar, as pointed above.

Period T as a function of P and B

The issue of how the period T is related with the representation with P decimal digits was studied by Grebogi and coworkers [?]. There they show that the period T scales with roundoff ϵ as $T \sim \epsilon^{-d/2}$ where d is the correlation dimension of the chaotic attractor. Nagaraj et al [?] studied the case of switching between two maps. They show that the period T of the compound map obtained by switching between two chaotic maps is higher than the period of each map and they found that a "random" switching improves the results. Here we considered sequential switching to avoid the use of another random variable, because it can include its own statistical properties in the time series. We studied decimal and binary numbers representations. Fig. ?? shows T vs P in semi logarithmic scale. A straight line can fit the points and has the expression $\log_{10} T = m \times P + b$ for decimal numbers and $\log_2 T = m \times B + b$ for binary numbers, where m is the slope and b is the y -intercept. Results for all considered maps are summarized in Table 4.1 and 4.2.

Cuadro 4.1: Period T as a function of P for the maps considered

map	m	b
TENT	0.436	-0.0705
LOG	0.422	0.0141
SWITCH	0.438	0.0276
EVEN	0.438	- 0.2734
ODD	0.438	- 0.2734

Cuadro 4.2: Period T as a function of B for the maps considered

map	m	b
TENT	-	-
LOG	0.494	-1.219
SWITCH	0.494	-0.871
EVEN	0.494	-1.871
ODD	0.494	-1.871

Results are compatible for those obtained in [?]. Switching between maps increase de period T but the skipping procedure decrease it esentially to one half.

4.2.5. Conclusions

In summary:

-
-
-

produces a non-monotonous evolution toward the floating point result. This result is relevant because it shows that increasing the precision is not always recommended.

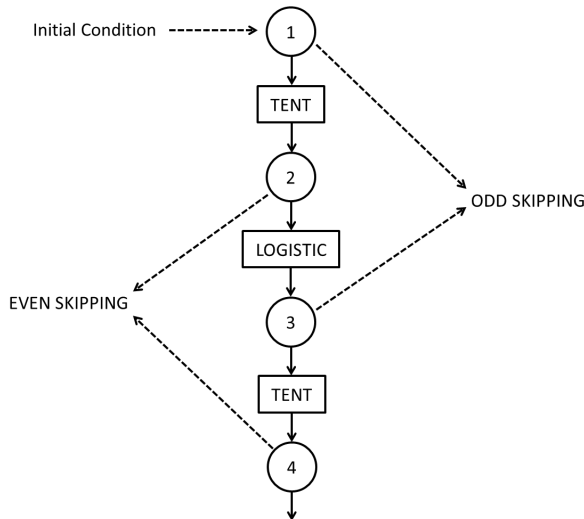


Figura 4.1: ZONA CH REHACER

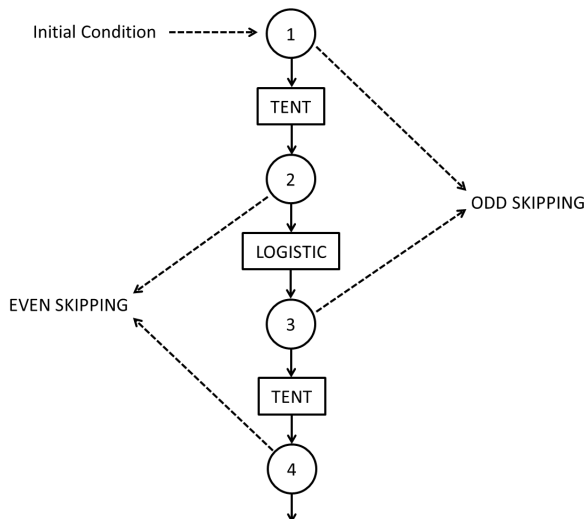


Figura 4.2: Sequential switching between Tent and Logistic maps. In the figure are also shown even and odd skipping strategies

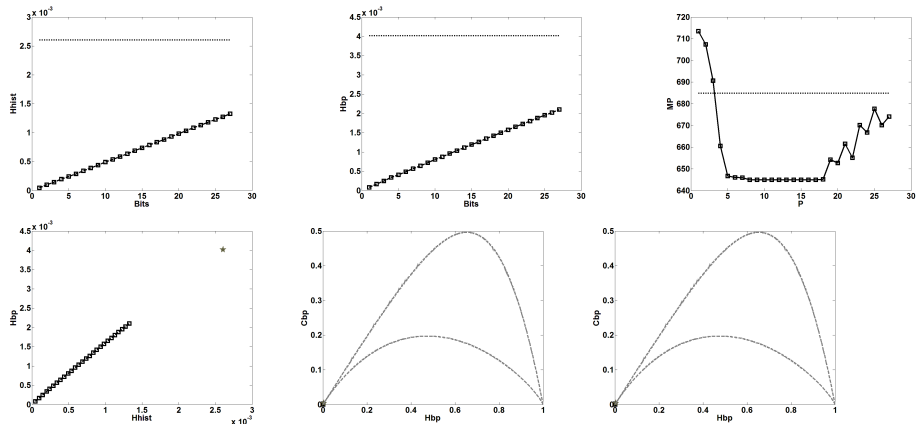


Figura 4.3: Statistical properties of the Tent map using different numerical representations. Figures (a) to(e) correspond to decimal representation: (a) H_{hist} vs P (b) H_{BP} vs P (c) Number of missing ordering patterns MP vs P . In Figures (a) to (c) dashed line correspond to floating point numbers. (d) representation in the H_{hist}, H_{BP} plane in the the decimal numerical system. The star represents the state for floating points numbers. (e) representation in the H_{BP}, C_{BP} plane. The star represents the state for floating points numbers. (f) representation in the H_{BP}, C_{BP} plane for binary numerical system. The star represents the state for floating points numbers.

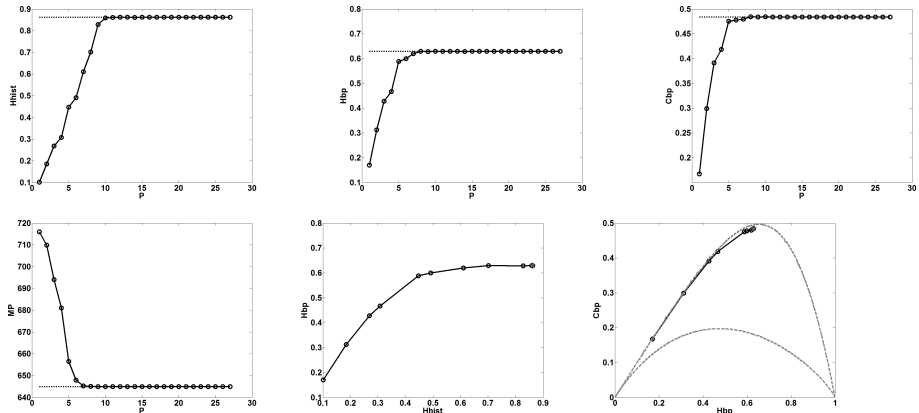


Figura 4.4: Statistical properties of the LOG map using different numerical representations. Figures (a) to(f) correspond to decimal representation: (a) H_{hist} vs P (b) H_{BP} vs P (c) C_{BP} vs P (d) Number of missing ordering patterns MP vs P . In Figures (a) to (d) dashed line correspond to floating point numbers. (d) representation in the H_{hist}, H_{BP} plane in the the decimal numerical system. The star represents the state for floating points numbers. (e) representation in the H_{hist}, H_{BP} plane. The star represents the state for floating point numbers; (f) representation in the H_{BP}, C_{BP} plane. The star represents the state for floating points numbers. (f) representation in the H_{BP}, C_{BP} plane for binary numerical system. The star represents the state for floating points numbers.

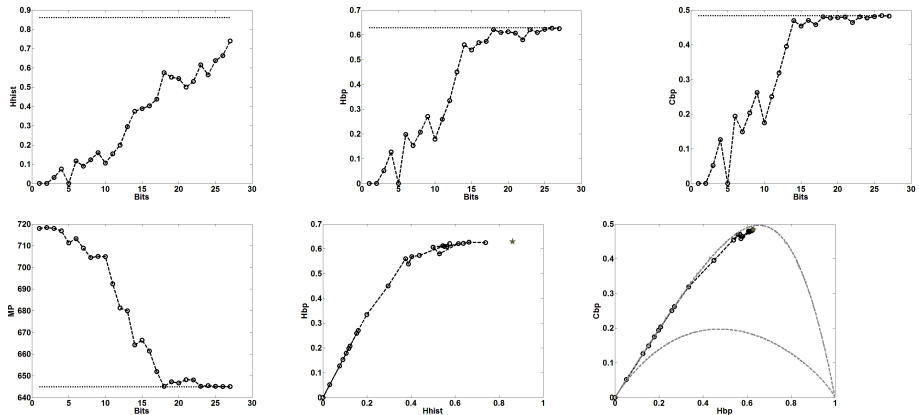


Figura 4.5: Statistical properties of the LOG map using binary representation: (a) H_{hist} vs P (b) H_{BP} vs P (c) C_{BP} vs P (d) Number of missing ordering patterns MP vs P . In Figures (a) to (d) dashed line correspond to floating point numbers. (d) representation in the H_{hist}, H_{BP} plane in the decimal numerical system. The star represents the state for floating points numbers. (e) representation in the H_{hist}, H_{BP} plane. The star represents the state for floating point numbers; (f) representation in the H_{BP}, C_{BP} plane. The star represents the state for floating points numbers. (f) representation in the H_{BP}, C_{BP} plane for binary numerical system. The star represents the state for floating points numbers.

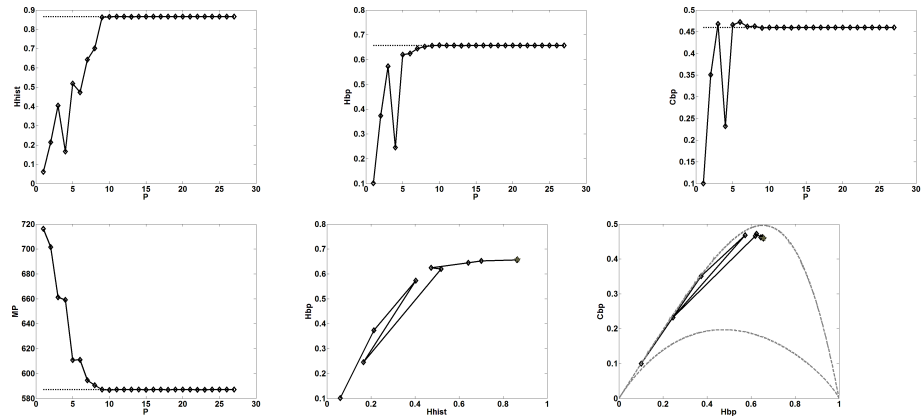


Figura 4.6: Statistical properties of the SWITCH map using decimal representation: (a) H_{hist} vs P (b) H_{BP} vs P (c) C_{BP} vs P (d) Number of missing ordering patterns MP vs P . In Figures (a) to (d) dashed line correspond to floating point numbers. (e) representation in the H_{hist}, H_{BP} plane in the the decimal numerical system. The star represents the state for floating points numbers. (f) representation in the H_{BP}, C_{BP} plane. The star represents the state for floating points numbers. (The star represents the state for floating points numbers).

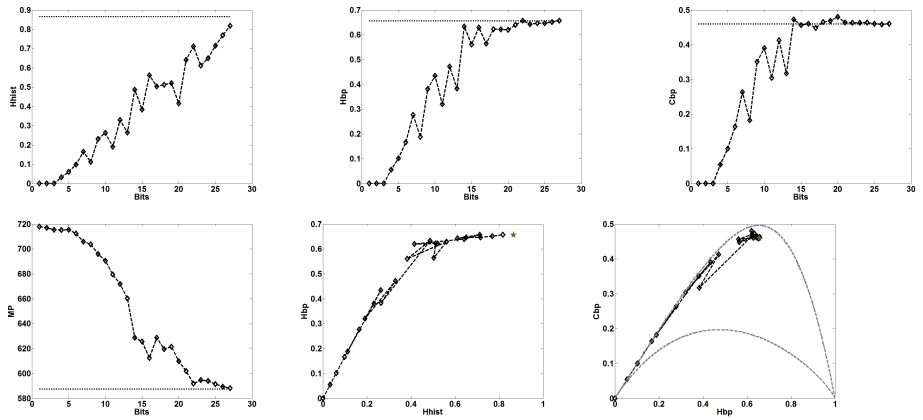


Figura 4.7: Statistical properties of the SWITCH map using binary representation: (a) H_{hist} vs P (b) H_{BP} vs P (c) C_{BP} vs P (d) Number of missing ordering patterns MP vs P . In Figures (a) to (d) dashed line correspond to floating point numbers. (e) representation in the H_{hist}, H_{BP} plane in the the binary numerical system. The star represents the state for floating points numbers. (f) representation in the H_{BP}, C_{BP} plane. The star represents the state for floating points numbers. (The star represents the state for floating points numbers).

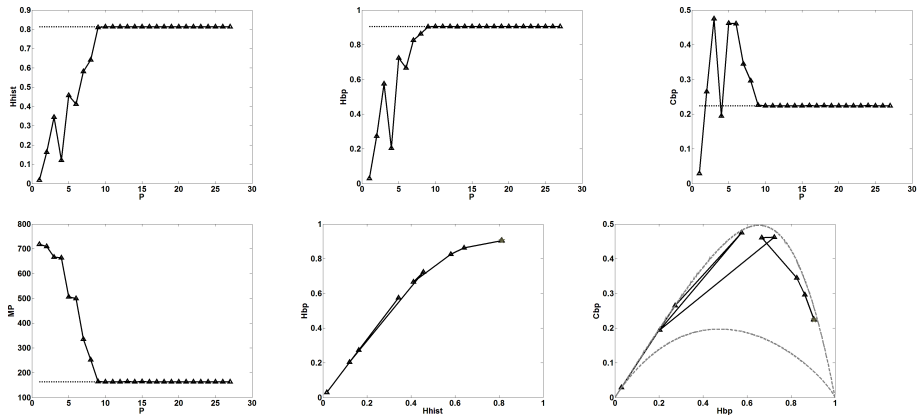


Figura 4.8: Statistical properties of EVEN, obtained by skipping the values in the odd position of the time series of SWITCH, using decimal representation: (a) H_{hist} vs P (b) H_{BP} vs P (c) C_{BP} vs P (d) Number of missing ordering patterns MP vs P . In Figures (a) to (d) dashed line correspond to floating point numbers. (e) representation in the H_{hist}, H_{BP} plane in the the decimal numerical system. The star represents the state for floating points numbers. (f) representation in the H_{BP}, C_{BP} plane. The star represents the state for floating points numbers.

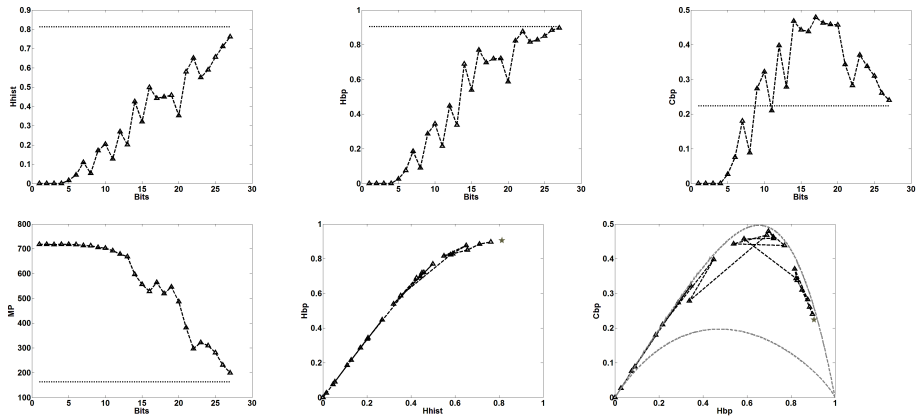


Figura 4.9: Statistical properties of EVEN, obtained by skipping the values in the odd position of the time series of SWITCH, using binary representation: (a) H_{hist} vs P (b) H_{BP} vs P (c) C_{BP} vs P (d) Number of missing ordering patterns MP vs P . In Figures (a) to (d) dashed line correspond to floating point numbers. (e) representation in the H_{hist}, H_{BP} plane in the the binary numerical system. The star represents the state for floating points numbers. (f) representation in the H_{BP}, C_{BP} plane. The star represents the state for floating points numbers.

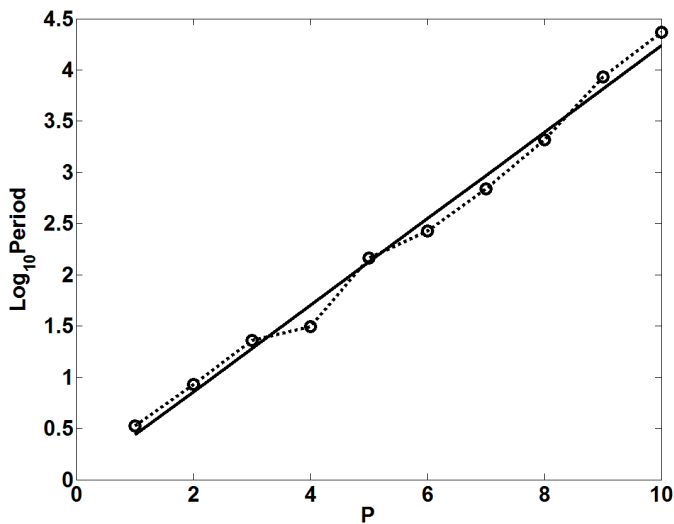


Figura 4.10: Period T as a function de number of decimal digits P for the LOG map.

Capítulo 5

Conclusiones

Terminé

Apéndice A

Field Programmable Gate Array (FPGA)

Cosas que distraen en la tesis.

Bibliografía